The influence of tidal heating on the Earth's thermal evolution along the dynamical history of the Earth-Moon system

Santiago Hernan Luna[1], Mauro Gabriel Spagnuolo[2], and Hugo Daniel Navone[3]

[1]Instituto de Estudios Andinos "Don Pablo Groeber" (IDEAN), Universidad de Buenos Aires - CONICET
[2]IDEAN, Universidad de Buenos Aires, Conicet.
[3]Facultad de Ciencias Exactas, Ingeniería y Agrimensura. Universidad Nacional de Rosario

November 23, 2022

Abstract

Several geological evidences, such as tidal rhythmites and bivalve shells, allow to track back the evolution paths of both the major semiaxis of the Moon's orbit and the Earth's spin rate. However, the data is scarce and with large uncertainty and the orbital evolution of the Moon is still controversial. The aim of this work is to evaluate how significant could have been the effect of bodily tides on the Earth's mantle thermal evolution. To this end, different thermal models of the Earth's interior were proposed. We explore plate tectonics and stagnant lid regimes. These models take into account both tidal and radiogenic heat sources. In order to compute tidal dissipation, we made use of three realistic rheological models of Earth mantle and proposed three different dynamical evolution paths for the lunar major semiaxis and terrestrial length of day. It was found that the impact of tidal interaction could have been specially appreciable on the first hundreds million of years of the Earth's history, provided that the mantle was at a higher temperature. In addition, we found that thermal evolution of Earth's interior is mainly controlled by the rheological behavior of the mantle, which controls the amount of tidal heat produced, and by the dynamical evolution of the Earth-Moon system.

The influence of tidal heating on the Earth's thermal evolution along the dynamical history of the Earth-Moon system

S. H. Luna[1], M. G. Spagnuolo[2], H. D. Navone[3,4]

[1]Instituto de Estudios Andinos "Don Pablo Groeber" (IDEAN). Universidad de Buenos Aires – CONICET. Intendente Güiraldes 2160, Ciudad Universitaria, Pabellón II, C1428EGA, Ciudad Autónoma de Buenos Aires, Argentina.
[2]Instituto de Estudios Andinos "Don Pablo Groeber" (IDEAN). Universidad de Buenos Aires – CONICET. Intendente Güiraldes 2160, Ciudad Universitaria, Pabellón II, C1428EGA, Ciudad Autónoma de Buenos Aires, Argentina. E-mail: mgspag@gmail.com
[3]Facultad de Ciencias Exactas, Ingeniería y Agrimensura. Universidad Nacional de Rosario. Av. Pellegrini 250, S2000BTP, Rosario, Argentina.
[4]Instituto de Física de Rosario (IFIR). CONICET – Universidad Nacional de Rosario. Bv. 27 de Febrero, S2000EKF, Rosario, Argentina.

Key Points:

- Geological evidences allow to track back a possible dynamical evolution path of the Earth-Moon system and to evaluate tidal heating.
- We found that tidal heating could have played a significant role in the Earth's thermal history.
- Our results suggest that the onset of plate tectonics may have occurred between 4.5 and 3.5 billion years in the past.

Corresponding author: Santiago Luna, santiagohluna@gmail.com

Abstract

Several geological evidences, such as tidal rhythmites and bivalve shells, allow to track back the evolution paths of both the major semiaxis of the Moon's orbit and the Earth's spin rate. However, the data is scarce and with large uncertainty and the orbital evolution of the Moon is still controversial. The aim of this work is to evaluate how significant could have been the effect of bodily tides on the Earth's mantle thermal evolution. To this end, different thermal models of the Earth's interior were proposed. We explore plate tectonics and stagnant lid regimes. These models take into account both tidal and radiogenic heat sources. In order to compute tidal dissipation, we made use of three realistic rheological models of Earth mantle and proposed three different dynamical evolution paths for the lunar major semiaxis and terrestrial length of day. It was found that the impact of tidal interaction could have been specially appreciable on the first hundreds million of years of the Earth's history, provided that the mantle was at a higher temperature. In addition, we found that thermal evolution of Earth's interior is mainly controlled by the rheological behavior of the mantle, which controls the amount of tidal heat produced, and by the dynamical evolution of the Earth-Moon system.

Plain Language Summary

We aim to try to answer the question of how could the Moon have influenced the onset of plate tectonics in our planet. In our work, we take under consideration the effect of bodily tides, i.e. the deformation of the Earth as a whole due to the gravitational attraction exerted by the Moon. This deformation heats the Earth's interior due to friction. We also take into account the heat generated by the decay of radioactive isotopes. These sources of heat are counteracted by thermal convection. The interaction between the heating and cooling mechanisms determines the time evolution of the internal temperatures of the Earth which, in turn, controls the lithosphere's thickness, which give clues when plate tectonics could have started. The evaluation of tidal heating depends on the combination of rotational period of the Earth and the orbital period of the Moon, which changed over time. We used geological data to obtain a possible evolution path of both periods. We found that tidal heating could have had a significant role in the early stages of Earth's thermal history and that the plate tectonics may started between 4.5 and 3.5 billion years in the past.

1 Introduction

Since its formation, the dynamical evolution of the Earth-Moon system was characterized by the progressive increase of the mutual distance between both members of the system, the probably rapid capture of the Moon in the spin-orbit resonance 1:1 (Makarov, 2013), and the gradual decrease of the angular spin rate of the Earth.

Several geological evidences offer clues about the possible evolution path of the Earth-Moon system, such as the one found in bivalve fossil records and in rocks called *tidal rhythmites*, which account for the tidal cycles (Williams, 2000; López de Azarevich & Azarevich, 2017). The stratified structure of these rocks are interpreted as variations in the sea level as a consequence of tidal interaction and, hence, the lunar cycle. The bivalve fossils growing cycles are interpreted as an evidence of the length of day (LOD). However, the data is scarce and with large uncertainty. In addition, the orbital evolution of the Moon is still controversial.

Rigorous analysis of the aforementioned evidences has allowed the estimation of variations in the length of the day, the orbital period of the Moon and the orbital period of the Earth around the Sun throughout time. This information serve as a "ground truth" for contrasting the theoretical models with empirical evidence, a fundamental procedure in natural sciences.

The main objective of this work is to evaluate how large could have been the impact of tidal heating, arising from bodily tides raised by the Moon, on the thermal evolution of the Earth. To that end, we developed different thermal models that includes an up-to-date expression for the rate of tidal heating or, in other words, the rate at which heat is produced due to internal dissipation within Earth's mantle.

The Darwin-Kaula formalism of Tidal Theory (Efroimsky & Makarov, 2013) offers a complete theoretical framework for the computation of the heat production rate due to internal dissipation excited by tidal loading.

Tidal interaction is originated by the deformation of a celestial body due to gravitational forces acting on it, exerted by other bodies. This deformation, in turn, modifies the gravitational field of the Earth, thus disturbing the orbital motion of the Moon and the LOD. Since the deformation depends on the rheology we investigate different rheological models (see the Supplementary information). We assume, on one hand, that the Earth is spherical with a concentric layered interior structure containing homogeneous core and mantle and, eventually, a lithosphere. On the other hand, the Moon is assumed to be a point mass distribution.

Thermal evolution of the Earth's interior is described by using simple parametric one-dimensional models of thermal convection. These models consider the boundary layer theory to describe heat transfer within both the Earth's core and mantle and are explained in detail in Section 2.

Later, the implementation of the aforementioned thermal model is explained in detail in Section 3, which also offers a discussion about the compatibility of observational data with the dynamic characteristics imposed by tidal interaction. Then, the results obtained from the numerical simulations carried out are presented and discussed in Section 4. Lastly, our conclusions are offered in Section 5.

2 Thermal evolution models of Earth's interior

As we have pointed out in Section 1, we model the Earth's interior as a two layers structure composed by the core and the mantle as shown in Figure 1. Two different regimes will be considered, namely the plate tectonics (PT) and the stagnant lid (SL). In the former, the Earth is assumed to be formed by the two aforementioned layers (Figure 1a). In the stagnant lid regime an extra layer is included in the thermal model representing a thick elastic lithosphere (Figure 1b).

The study of the time evolution of the temperatures inside the Earth makes use of the continuity equation for energy flow and energy balance within both the core and the mantle. On geological time scales, the dominant heat transfer mechanism is convection (Stacey & Davis, 2008; Turcotte & Schubert, 2014). In this sense, we will consider simple parametric one-dimensional models to describe the temporal evolution of the mean temperatures of both the core and the mantle due to convection. These models, for both the plate tectonics and stagnant lid regimes, will be presented in the following subsections.

Let us then consider the continuity equation expressing the principle of energy conservation:

$$\frac{\partial u}{\partial t} + \nabla \cdot \mathbf{q} = \varrho\left(\mathbf{r}, t\right), \tag{1}$$

where u is the energy density, in other words the amount of energy per unit volume, and $\mathbf{q}$ is the heat flux vector, whose magnitude is equal to the amount of energy per unit area and unit time that crosses an specified surface, its direction is perpendicular

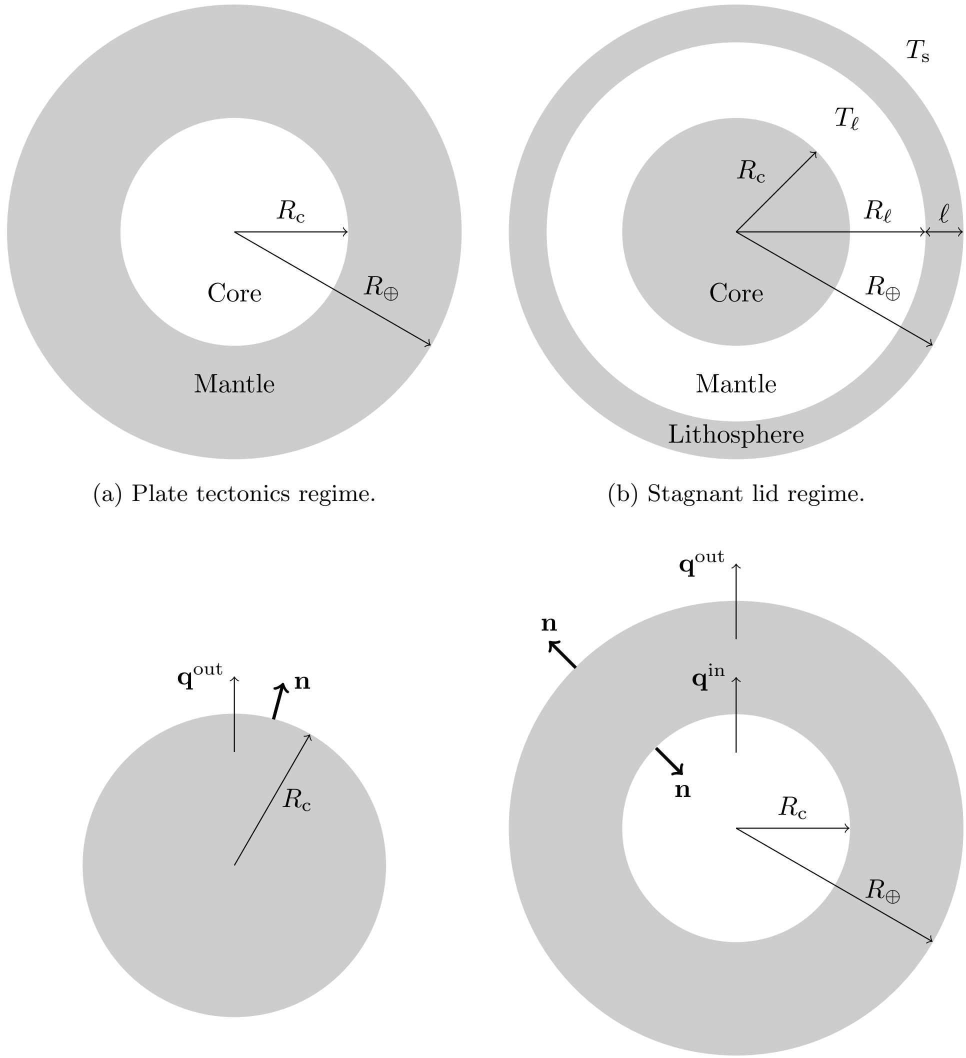

(a) Plate tectonics regime.

(b) Stagnant lid regime.

(c) Heat flow through core's surface.

(d) Heat flow through inner and outer surfaces of the mantle.

Figure 1: Schematics of the Earth's interior structure for both the plate tectonics regime (a) and the stagnant lid regime (b). Heat flow through the core surface (c) and the inner and outer surfaces of the mantle (d).

to that surface and its sense is outwards. In addition, $\varrho(\mathbf{r}, t)$ is the heat production rate per unit volume which, in principle, could be a function of the position and time.

As the principle of energy conservation implies that energy is neither destroyed nor created, but only transformed from one type to another, by using the term "sources" we simply mean *sources of thermal energy*. In this work we will consider two of them, namely that from the decay of radioactive nuclides and tidal interaction.

A special form of Equation (1) is obtained when there are no sources:

$$\frac{\partial u}{\partial t} + \nabla \cdot \mathbf{q} = 0. \tag{2}$$

The particular functional form of $\varrho\,(\mathbf{r},t)$ will then depend on the source or sources considered. For the Earth, we will assume that heat sources are uniformly distributed in the mantle and we will neglect the presence of sources in the core and in the lithosphere. In this sense, Equation (2) will allow us to derive the differential equation giving the time evolution of the core's temperature, while the equation describing the time evolution of the mantle's temperature will be obtained from Equation (1).

If we assume that changes in the amount of internal energy per unit volume Δu is only due to temperature changes (ΔT), in other words we neglect phase transitions, then Δu is given by:

$$\Delta u = \rho\, c\, \Delta T, \tag{3}$$

where ρ is the density and c is the specific heat. If we now divide both members of Equation (3) by the time interval during which the change of the temperature and, consequently, the change in the internal energy density takes place, and then we take the limit when $\Delta t \to 0$, we obtain:

$$\frac{\partial u}{\partial t} = \rho\, c\, \frac{\partial T}{\partial t}. \tag{4}$$

The partial time derivative is considered due to the possibility that u and T depend on other variables like the point at which they are measured.

Let us consider first the thermal evolution of the Earth's core. In order to obtain the corresponding differential equation giving the time derivative of core's temperature, we should insert Equation (4) into Equation (2), which leads to:

$$\rho\, c\, \frac{\partial T}{\partial t} + \nabla \cdot \mathbf{q} = 0. \tag{5}$$

Then we should integrate over the whole volume of the core. Certainly, core's physical parameters, such as its density and specific heat, as well as its temperature, can vary both temporally and spatially. However, as we want to track the time evolution of core's mean temperature, $\langle T \rangle_{\mathrm{c}}$, we will take the mean values of its density and specific heat and will assume that $\langle \rho \rangle_{\mathrm{c}}$ and $\langle c \rangle_{\mathrm{c}}$ are constant in time. Thus, the result of the volume integral of the first term on the left hand side of Equation (5) is equal to the product of $\rho\, c\, \partial T/\partial t$ and the core's volume. In addition, the volume integral of the second term on the left hand side of Equation (5) is transformed into a surface integral by virtue of the divergence theorem, which should be evaluated on the core's surface. If we assume that heat flows outwards only in the radial direction, as shown in Figure 1c, then $\mathbf{q}^{\mathrm{out}} \cdot \mathbf{n} = q^{\mathrm{out}}$. Thus, Equation (5) can be rewritten as:

$$\rho_{\mathrm{c}}\, c_{\mathrm{c}}\, \frac{\mathrm{d}\,\langle T \rangle_{\mathrm{c}}}{\mathrm{d}t}\, V_{\mathrm{c}} + q^{\mathrm{out}}(t)\, A_{\mathrm{c}} = 0, \tag{6}$$

where V_{c} and A_{c} are the volume and external surface area of the core, respectively. Equation (6) can also be expressed as:

$$\frac{\mathrm{d}\,\langle T \rangle_{\mathrm{c}}}{\mathrm{d}t} = -\frac{3}{\rho_{\mathrm{c}}\, c_{\mathrm{c}}} \frac{q^{\mathrm{out}}(t)}{R_{\mathrm{c}}}. \tag{7}$$

It should be pointed out that in Equations (6) and (7) we omitted the mean value symbol for the core's density and specific heat for the sake of simplicity.

Concerning the thermal evolution of the mantle, an analogous reasoning is followed. We begin with Equation (1) in which we insert Equation (4) and then we integrate on both members over the volume of the mantle. Then, by assuming that the mean density, the specific heat, and the temperature of the mantle, as well as the rate of heat production over its volume, are homogeneous the volume integral of the first term on the left hand side of Equation (1) is equal to $\rho_{\mathrm{m}}\, c_{\mathrm{m}} \frac{\mathrm{d}\langle T \rangle_{\mathrm{m}}}{\mathrm{d}t}\, V_{\mathrm{m}}$, where ρ_{m} and c_{m} are the mean density and mean specific heat of the mantle, respectively, and

V_m is the mantle's volume. In addition, we have assumed that mantle temperature depends only on time and, consequently, we track the time evolution of the mean mantle's temperature, $\langle T\rangle_\mathrm{m}$.

The volume integral of the second term on the left hand side of Equation (1) is also transformed into a surface integral by virtue of the divergence's theorem. As can be noted in Figure 1d, the Earth's mantle is enclosed by two concentric spherical surfaces, the inner of radius R_c and the outer of radius $R_\oplus$. This implies that the aforementioned surface integral must be split into two separate surface integrals corresponding to each limiting surface.

Analogously to the case of the Earth's core, we assume that heat flows outwards only in the radial direction and that it depends only on time. Hence, we have that $\mathbf{q}^\mathrm{in} = q^\mathrm{in}(t)\,\mathbf{n}$ and $\mathbf{q}^\mathrm{out} = q^\mathrm{out}(t)\,\mathbf{n}$. Thus, $\mathbf{q}^\mathrm{in}\cdot\mathbf{n} = -q^\mathrm{in}(t)$ and $\mathbf{q}^\mathrm{out}\cdot\mathbf{n} = q^\mathrm{out}(t)$. As result, Equation (1) is expressed as:

$$\rho_\mathrm{m}\, c_\mathrm{m}\,\frac{\mathrm{d}\,\langle T\rangle_\mathrm{m}}{\mathrm{d}t}\,V_\mathrm{m} - q^\mathrm{in}\,A^\mathrm{in} + q^\mathrm{out}A^\mathrm{out} = \varrho_\mathrm{m}(t)V_\mathrm{m}, \tag{8}$$

where A^in and A^out are the areas of the inner and outer spherical surfaces, respectively.

Equation (8) can be reshaped in a form similar to Equation (7). On one hand, the mantle's volume is:

$$V_\mathrm{m} = \frac{4}{3}\pi\,R_\oplus^3\left(1-x^3\right), \tag{9}$$

where

$$x = \frac{R_\mathrm{c}}{R_\oplus}. \tag{10}$$

On the other hand, the areas of the inner and outer limiting surfaces are:

$$A^\mathrm{in} = 4\,\pi\,R_\mathrm{c}^2, \tag{11a}$$
$$A^\mathrm{out} = 4\,\pi\,R_\oplus^2. \tag{11b}$$

By inserting Equation (9) and (11) into Equation (8), we obtain:

$$\frac{\mathrm{d}\,\langle T\rangle_\mathrm{m}}{\mathrm{d}t} = \frac{1}{\rho_\mathrm{m}\,c_\mathrm{m}}\left(3\frac{\left[x^2 q_\mathrm{m}^\mathrm{in}(t) - q_\mathrm{m}^\mathrm{out}(t)\right]}{R_\oplus\left(1-x^3\right)} + \varrho_\mathrm{m}(t)\right). \tag{12}$$

Now that we have derived Equations (7) and (12), which give the time evolution of the core and mantle of the Earth, respectively, the next step is to obtain the corresponding expressions of the outgoing thermal flux from the core and those entering into and outgoing from the mantle.

The general expression of the heat flux due to convection is:

$$q^\mathrm{conv} = k\frac{\Delta T}{d}, \tag{13}$$

where

$$d = \left(\frac{\mathrm{Ra_{cr}}\,\kappa\,\eta}{2^4\alpha\,\rho\,g\,\Delta T}\right)^{\frac{1}{3}}. \tag{14}$$

See the Supplementary information for a detailed derivation of Equations (13) and (14). Insertion of Equation (14) into Equation (13) leads to:

$$q^\mathrm{conv} = k\left(\frac{2^4}{\mathrm{Ra_{cr}}}\frac{\alpha\,\rho\,g\,\Delta T}{\kappa\,\eta}\right)^{\frac{1}{3}}\Delta T. \tag{15}$$

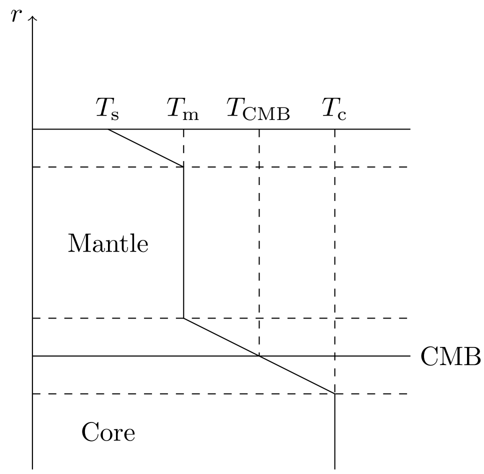

Figure 2: Vertical temperature profile corresponding to the plate tectonics regime due to convection. The earth is assumed to be internally differentiated into two layers, namely the core and the mantle. Both are divided by an imaginary spherical surface called core-mantle boundary (CMB).

The heat flux outgoing from the core will have the same form in both the plate tectonics and stagnant lid regimes. For that reason, we consider its expression here. Taking into account Figure 2 and Equation (15), we find that:

$$q_\mathrm{c}^\mathrm{out}(t) = k_\mathrm{c} \left(\frac{2^4}{\mathrm{Ra}_\mathrm{cr}} \frac{\alpha_\mathrm{c}\, g_\mathrm{c}}{\kappa_\mathrm{c}\, \nu_\mathrm{c}} \right)^{\frac{1}{3}} \left[\langle T \rangle_\mathrm{c}(t) - T_\mathrm{CMB}(t) \right]^{\frac{4}{3}} , \tag{16}$$

where

$$\nu = \frac{\eta}{\rho}$$

is the kinematic viscosity, T_CMB is the mean temperature at the core-mantle boundary (CMB) and $\langle T \rangle_\mathrm{c}$ is the mean temperature of the core, which is obtained from Equation (7), and correspond to the isothermal temperature of the thermal convection model considered in our work.

The heat flux incoming into the mantle has the same functional form for both the considered regimes pointed out above as well. By taking into account Figure 2 and Equation (15) once again, we arrive to:

$$q_\mathrm{m}^\mathrm{in}(t) = k_\mathrm{m} \left(\frac{2^4}{\mathrm{Ra}_\mathrm{cr}} \frac{\alpha_\mathrm{m}\, \rho_\mathrm{m}\, g_\mathrm{m}}{\kappa_\mathrm{m}\, \eta_\mathrm{m}} \right)^{\frac{1}{3}} \left[T_\mathrm{CMB}(t) - \langle T \rangle_\mathrm{m}(t) \right]^{\frac{4}{3}} , \tag{17}$$

where $\langle T \rangle_\mathrm{m}$ is the mean (isothermal) temperature of the mantle. The mean temperature at the CMB is obtained by equating the right hand side of Equations (16) and (17), leading to:

$$T_\mathrm{CMB} = \frac{\langle T \rangle_\mathrm{m} + \varphi\, \langle T \rangle_\mathrm{c}}{1+\varphi} \tag{18}$$

where

$$\varphi = \left(\frac{k_\mathrm{n}}{k_\mathrm{m}} \right)^{\frac{3}{4}} \left(\frac{\alpha_\mathrm{n}\, g_\mathrm{n}\, \kappa_\mathrm{m}\, \eta_\mathrm{m}}{\alpha_\mathrm{m}\, \rho_\mathrm{m}\, g_\mathrm{m}\, \kappa_\mathrm{n}\, \nu_\mathrm{n}} \right)^{\frac{1}{4}} . \tag{19}$$

It worth to point out that mantle's dynamical viscosity depends on the T_m according to Equation (43).

2.1 Thermal evolution in the plate tectonics regime

The expression of the outgoing thermal flux from the mantle is (see Supplementary material):

$$q_{\mathrm{m}}^{\mathrm{out}}(t) = k_{\mathrm{m}} \left(\frac{2^4}{\mathrm{Ra}_{\mathrm{cr}}} \frac{\alpha_{\mathrm{m}}\, \rho_{\mathrm{m}}\, g_{\mathrm{m}}}{\kappa_{\mathrm{m}}\, \eta_{\mathrm{m}}} \right)^{\frac{1}{3}} \left[\langle T \rangle_{\mathrm{m}}(t) - T_{\mathrm{s}} \right]^{\frac{4}{3}}, \tag{20}$$

where T_{s} is the temperature at the Earth surface, which is assumed to be constant.

Equations (16), (17), (18), (19), (20) and (43), together with Equations (7) and (12), allow to perform the numerical simulations of the thermal evolution of Earth's interior once the particular form of ϱ_{m} has been considered. The latter issue will be approached in Section 3.

2.2 Thermal evolution in the stagnant lid regime

The thermal evolution model of the stagnant lid regime includes Equations (16), (17), (18), (19) and (7) without modifications. However, Equations (12) and (20) have to be refined. The main difference lies on the consideration of an external elastic lid, the lithosphere, ranging from the external surface of the mantle up to the Earth surface, of thickness ℓ (see Figure 1b). The lithosphere is assumed to be an external stagnant lid of the Earth in the sense that it has no lateral motions, but its thickness changes on time.

The equation giving the time evolution of the lithosphere's thickness is (Schubert et al., 1979; Spohn, 1991; Grott & Breuer, 2008; Stamenković et al., 2012):

$$\rho_{\mathrm{m}} c_{\mathrm{m}} \left(\langle T \rangle_{\mathrm{m}} - T_\ell \right) \frac{\mathrm{d}\ell}{\mathrm{d}t} = q_\ell - q_{\mathrm{m}}^{\mathrm{out}}, \tag{21}$$

where T_ℓ and q_ℓ are the temperature and thermal flux at the base of the lithosphere, respectively. Thus, provided that $\langle T \rangle_{\mathrm{m}}$ will always be grater that T_ℓ, the lithosphere's thickness will grow or decrease according to if q_ℓ is grater or lower than $q_{\mathrm{m}}^{\mathrm{out}}$, respectively.

The expression of the outgoing thermal flux of the mantle is slightly different from that of Equation (20). As the lithosphere is no longer part of the convecting mantle, as in the plate tectonics regime, the upper bound temperature is not T_{s}, but T_ℓ. In consequence, we have:

$$q_{\mathrm{m}}^{\mathrm{out}}(t) = k_{\mathrm{m}} \left(\frac{2^4}{\mathrm{Ra}_{\mathrm{cr}}} \frac{\alpha_{\mathrm{m}}\, \rho_{\mathrm{m}}\, g_{\mathrm{m}}}{\kappa_{\mathrm{m}}\, \eta_{\mathrm{m}}} \right)^{\frac{1}{3}} \left[\langle T \rangle_{\mathrm{m}}(t) - T_\ell(t) \right]^{\frac{4}{3}}. \tag{22}$$

The time dependence of the temperature at the base of the lithosphere is due to its dependence on the mean mantle's temperature, provided that it will be computed following the work by Stamenković et al. (2012):

$$T_\ell(t) = \langle T \rangle_{\mathrm{m}}(t) - \frac{\ln 10\, R_{\mathrm{gas}}\, \langle T \rangle_{\mathrm{m}}^2(t)}{E^*}. \tag{23}$$

The expression of the thermal flux entering the lithosphere (q_ℓ) is given by:

$$q_\ell = k_{\mathrm{m}} \frac{(T_\ell - T_{\mathrm{s}})}{\ell}, \tag{24}$$

where we assume that the thermal conductivity of the lithosphere is equal to that of the mantle. We may point out that both Equation (13) and (24) were derived assuming steady state regime of heat transport, which is described by $\nabla \cdot \mathbf{q} = 0$. It arises the question about the validity of this approach since we are considering time evolution of the internal temperatures of the Earth. However, as is pointed out by

Stamenković et al. (2012), the aforementioned approximation can be justified by the fact that relaxation time of the lithosphere is typically on the order of 100 Ma. In contrast, the relaxation time of the mantle is of the order of few Ga, in other words, the latter is much grater that the former.

Another important difference between the thermal model in the plate tectonics regime and that of the stagnant lid regime, lies on the fact that as the lithosphere thickness changes on time, also change both the mantle's and lithosphere's volumes. The change in the mantle's volume affects the expression of the time evolution of the $\langle T \rangle_{\mathrm{m}}$.

The volume of the mantle in the stagnant lid regime is given by:

$$\begin{aligned} V_{\mathrm{m}} &= \frac{4}{3}\pi \left[(R_{\oplus} - \ell)^3 - R_{\mathrm{n}}^3 \right], \\ &= \frac{4}{3}\pi R_{\oplus}^3 \left(y^3 - x^3 \right), \end{aligned} \tag{25}$$

where we have defined y as:

$$y = 1 - \frac{\ell}{R_{\oplus}}. \tag{26}$$

Analogously, the surface area of the mantle is computed as:

$$A_{\mathrm{m}} = 4\,\pi\,R_{\oplus}^2 y^2. \tag{27}$$

Bearing in mind Equations (25) and (26), by a reasoning similar to that leading to Equation (12), we arrive at:

$$\frac{\partial \langle T \rangle_{\mathrm{m}}}{\partial t} = \frac{1}{\rho_{\mathrm{m}}\,c_{\mathrm{m}}} \left(3\frac{\left[x^2 q_{\mathrm{m}}^{\mathrm{in}}(t) - y^2 q_{\mathrm{m}}^{\mathrm{out}}(t) \right]}{R_{\oplus}\left(y^3 - x^3 \right)} + \varrho_{\mathrm{m}}(t) \right). \tag{28}$$

Thus, the equations governing the thermal evolution in the stagnant lid regime are Equations (7) and (28) together with Equations (10), (16), (17), (18), (19), (21), (22), (23), (26) and (43).

It worth to note that Equation (12) can be obtained from Equation (28) by setting $y = 1$ or, equivalently, $\ell = 0$. This means that either there is no lithosphere at all or we are assuming that the lithosphere is part of the conductive lid of the convecting mantle as in Subsection 2.1.

2.3 Heat sources

The functional form of the heat production rate per unit volume and per unit time depends on the heat sources assumed to be present in the Earth's mantle. It worth to recall that we assume that heat sources are uniformly distributed in the mantle. In our work, we will take into account two sources of heat, namely the heat produced by the decay of radioactive isotopes and tidal heating.

On Earth, the most thermally relevant isotopes Uranium (235 and 238), Thorium and Potassium. On the other hand tidal heating is originated by internal friction within the tidally loaded Earth's mantle.

If heat is produced only by the decay of radioactive isotopes, then we have that:

$$\varrho_{\mathrm{m}}(t) = \rho_{\mathrm{m}}\,H(t). \tag{29}$$

where $H(t)$ is given by Turcotte and Schubert (2014) and it is reproduced in the Supplementary material.

However, if we assume that heat is produced by both the decay of radioactive elements and tidal heating, then $\varrho_{\mathrm{m}}(t)$ is given by:

$$\varrho_{\mathrm{m}}(t) = \rho_{\mathrm{m}}\, H(t) + \frac{\langle P\rangle_{\mathrm{m}}^{\mathrm{tide}}}{V_{\mathrm{m}}}, \tag{30}$$

where $\langle P\rangle_{\mathrm{m}}^{\mathrm{tide}}$ is the mean tidal heating rate in the Earth's mantle. The formula that we will use to compute the aforementioned quantity was developed by Efroimsky and Makarov (2014). However, that formula gives the mean tidal heating rate over the whole volume of the considered body, the Earth in our case. Still, we can use the expression by Efroimsky and Makarov (2014) taking into account that both tidal heating rates are related by (Renaud & Henning, 2018):

$$\frac{\langle P\rangle_{\mathrm{m}}^{\mathrm{tide}}}{V_{\mathrm{m}}} = \frac{\langle P\rangle_{\oplus}^{\mathrm{tide}}}{V_{\oplus}}, \tag{31}$$

where $\langle P\rangle_{\oplus}^{\mathrm{tide}}$ is given by:

$$\begin{aligned}\langle P\rangle_{\oplus}^{\mathrm{tide}} = \frac{G\, M_{☾}^{2}}{a} \sum_{l=2}^{\infty} \left(\frac{R_{\oplus}}{a}\right)^{2l+1} \sum_{m=0}^{l} \frac{(l-m)!}{(l+m)!}\,(2-\delta_{0m}) \\ \times \sum_{p=0}^{l} F_{lmp}^{2}(i) \sum_{q=-\infty}^{\infty} G_{lpq}^{2}(e)\, \omega_{lmpq}\, K_{\mathrm{I}}\left(l, \omega_{lmpq}\right),\end{aligned} \tag{32}$$

where G is the gravitation constant, $M_{☾}$ is the mass of the Moon, $R_{\oplus}$ is the mean Earth radius, a is the major semiaxis, δ_{0m} is the Kronecker delta distribution, $F_{lmp}(i)$ and $G_{lpq}(e)$ are the inclination (Gooding & Wagner, 2008) and eccentricity (Giacaglia, 1976) functions, respectively.

The factor $K_{\mathrm{I}}\left(l, \omega_{lmpq}\right)$ describes the rheological response of Earth, i.e. the modification of its gravitational field due to the deformation caused by the gravitational attraction forces exerted by the Moon, and is given by:

$$K_{\mathrm{I}}(l, \omega_{lmpq}) = -\frac{3}{2}\frac{1}{l-1}\frac{B_l\, \Im\left[\bar{J}(\chi)\right] \operatorname{sgn}\left(\omega_{lmpq}\right)}{\left(\Re\left[\bar{J}(\chi)\right] + B_l\right)^2 + \left(\Im\left[\bar{J}(\chi)\right]\right)^2}, \tag{33}$$

where $\Re\left(\bar{z}\right)$ and $\Im\left(\bar{z}\right)$ are the real and imaginary parts of the complex number $\bar{z}$, respectively, and χ_{lmpq} are the physical tidal frequencies which are defined through:

$$\chi_{lmpq} = \left|\omega_{lmpq}\right|, \tag{34}$$

where the tidal modes ω_{lmpq} are given by:

$$\omega_{lmpq} = (l-2p)\,\dot{\omega} + (l-2p+q)\,\dot{\mathcal{M}} + m\left(\dot{\Omega} - \dot{\theta}\right), \tag{35}$$

where $\dot{\mathcal{M}}$, $\dot{\omega}$ and $\dot{\Omega}$ are the time rates of the mean anomaly $\mathcal{M}$, the argument of perigee ω and the longitude of ascending node Ω (Efroimsky, 2012; Efroimsky, 2015). The latter two angles, as well as the inclination of the Moon's orbital plane i, are defined with respect to the Earth's equatorial plane. In many applications $\dot{\omega} \approx 0$ and $\dot{\Omega} \approx 0$ while $\dot{\mathcal{M}} \approx n$. Consequently the approximation

$$\omega_{lmpq} \approx (l-2p+q)\, n - m\,\dot{\theta}, \tag{36}$$

is generally valid and frequently used in the specialized literature. In Equation (36), n is the mean orbital frequency which for the unperturbed two-body problem is defined by the mathematical expression of Kepler's third law:

$$G\left(M_{\oplus} + M_{☾}\right) = n^2 a^3, \tag{37}$$

where $M_\oplus$ is the mass of the Earth. In addition, B_l is given by:

$$B_l = \frac{R_\oplus \left(2l^2 + 4l + 3\right)}{l\, G\, M_\oplus\, \rho_\oplus}, \tag{38}$$

where $\rho_\oplus$ is the mean density of the Earth. Lastly, $\bar{J}(\chi)$ is the complex creep-response or complex compliance function (Efroimsky, 2012; Efroimsky, 2015), which is defined through:

$$\bar{J}(\chi) = \int_0^\infty \dot{J}(t-t') \exp\left[-\mathrm{i}\chi(t-t')\right] \mathrm{d}t', \tag{39}$$

where the over-dot means differentiation with respect to t' and $\mathrm{i} = \sqrt{-1}$ is the imaginary unit. The particular form of the kernel $J(t-t')$ depends on the particular rheological model considered. However, it is generally given by:

$$J(t-t') = J(0)\, \Theta(t-t') + \text{viscous and hereditary terms}, \tag{40}$$

where $J(0)$ is the instantaneous value of the compliance which, in its turn, is the reciprocal value of the instantaneous rigidity $\mu(0)$, and $\Theta(t-t')$ is the Heaviside step function (Efroimsky, 2012).

2.4 Mantle viscosity

The dynamic viscosity, η, of the mantle depends, in general terms, on the temperature (T) and pressure (P) (Valencia et al., 2006; Henning et al., 2009; Stamenković et al., 2012). The functional form of this dependence is usually expressed in the form of Arrhenius' law:

$$\eta(T,P) = b \exp\left(\frac{E^* + P\, V^*_{\mathrm{eff}}\,(P)}{R_{\mathrm{gas}} T}\right), \tag{41}$$

where b is a constant, E^* and V^*_{eff} are the energy and effective volume of activation, respectively, and R_{gas} is the Universal constant of ideal gases.

As can be seen in Equation (41), the activation energy describes the coupling between viscosity and temperature, while the effective activation volume describes the coupling between pressure and viscosity. For reasons of simplicity, only the dependence of viscosity on temperature will be considered. In this sense, we set $V^*_{\mathrm{eff}} = 0$ and, consequently, Equation (41) is written as:

$$\eta(T) = b \exp\left(\frac{E^*}{R_{\mathrm{gas}} T}\right). \tag{42}$$

Following Stamenković et al. (2012), the latter equation can be rewritten in a more convenient way by considering a viscosity reference value corresponding to a temperature reference value, i.e. $\eta_{\mathrm{ref}} = \eta(T_{\mathrm{ref}})$. In this way the constant b can be eliminated and Eq (42) becomes:

$$\eta(T) = \eta_{\mathrm{ref}} \exp\left[\frac{E^*}{R_{\mathrm{gas}}}\left(\frac{1}{T} - \frac{1}{T_{\mathrm{ref}}}\right)\right]. \tag{43}$$

3 Model set up and implementation

This section is dedicated to discuss relevant details on the geological evidence, which allows the estimation of the tidal heating rate. In addition, we also present details concerning the numerical implementation of the thermal models we consider in our work, including the initial conditions and the assumed values of the parameters.

3.1 Geological evidences of the dynamical evolution of the Earth-Moon system

Detailed studies of a special type of rocks, called tidal rhythmites, and of bivalve shells have allowed the estimation of the time evolution of the rotational period of the

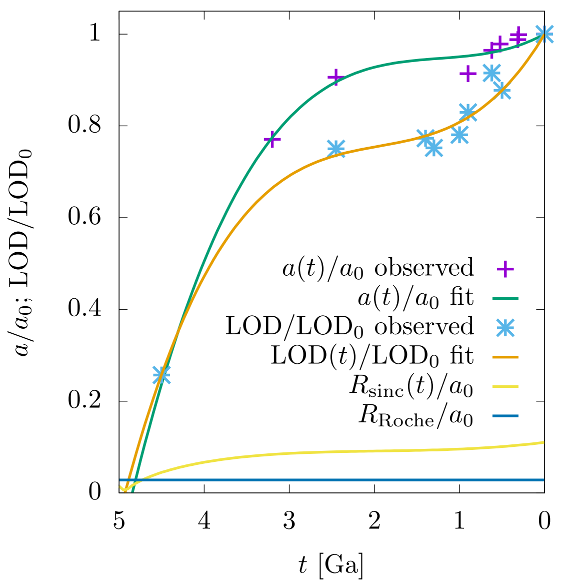

Figure 3: Normalized values of the major semiaxis of the lunar orbit and of the terrestrial length of day, estimated by studying the record of tidal cycles present in tidal rhythmites rocks, (dots) along the Earth's history. The corresponding polynomial fits of degree three are also shown, as well as the time evolution of the radius of the synchronous orbit, $R_{\rm sinc}/a_0$, and the Roche limit $R_{\rm Roche}/a_0$.

Earth and the orbital period of the Moon. In Figure 3, the estimated values of the major semiaxis (a) of the Moon's orbit with respect to the Earth and the length of day (LOD) of the latter are shown as a function of time during the Earth's history. Both data sets are normalized with respect to their current values, a_0 and LOD$_0$, respectively. The values of a were taken from the work by López de Azarevich and Azarevich (2017), while those of the LOD were gathered from the works by Williams (2000) and Spalding and Fischer (2019).

In addition, in Figure 3 the plots of the normalized radius of the synchronous orbit, $R_{\rm sinc}/a_0$, and the Roche limit, $R_{\rm Roche}/a_0$, are also included in order to show that the dynamical evolution of the Earth-Moon system, obtained from the geological evidences mentioned above, is consistent with the dynamical constraints imposed by tidal theory (Murray & Dermott, 1999).

In order to compute tidal dissipation rate as a function of time, along the dynamical history of the Earth-Moon system, we fit both data set with third degree polynomials. The main reason behind this choice is that a third degree polynomial is the simplest model that better fits the available data. Particularly, such polynomials represent the apparent change of concavity in the plot of the data. Interestingly, if we take the time derivative of the polynomial that fits the values of the major semiaxis along time, and evaluate it at the present, we find that it lies within the uncertainty of the current accepted value of the time rate of lunar recession measured by Lunar Laser Ranging (LLR) experiments (Bills & Ray, 1999). Thus, we obtain the major semiaxis of the lunar orbit and the Earth's spin rate as smooth functions of time and, consequently, we can evaluate tidal modes by using Equation (36) where the mean motion n is computed through Equation (37).

3.2 Thermal model set up

The tables with the values of all the parameters necessary to perform the required numerical computations are available at the Supplementary information. These includes the rheological parameters, such as the mean rigidity of the Earth's mantle μ, the reference shear viscosity η_{ref} (at the reference temperature T_{ref}), the activation energy E^* and the Andrade parameter α. In addition, the parameters and its respective assumed values for the evaluation of the time derivatives of the Earth's core and mantle temperatures, given in Equations (7), (12) and (28), are also available.

In order to evaluate the time rates of tidal heating, which are expressed infinite series over the l and q indexes, that is the right hand side of Equation (32), we need to truncate those series.

As can be noted in Equation (32), the leading terms of the corresponding expansions are of order $(R_\oplus/a)^5$ while the next to leading order term is of order $(R_\oplus/a)^7$. Currently, $R_\oplus/a_0 \approx 0.016$. However, near the origin of the Earth-Moon system the major semiaxis was about $0.3a_0$. Thus, the initial value of $R_\oplus/a \approx 0.055$. In consequence, $(R_\oplus/a)^5 \approx 5 \times 10^{-7}$ while $(R_\oplus/a)^7 \approx 1.55 \times 10^{-9}$. In other words, terms with $l = 3$ are at least two orders of magnitude lesser than those of the leading terms. We performed several numerical experiments comparing results using terms up to $l = 2$ and $l = 3$ in order to assess if appreciable differences appear between both sets of results. Even though differences are naturally expected, we however found that these differences are small enough to be considered negligible. Consequently, we can safely keep terms up to $l = 2$, obtaining simpler expressions of Equation (32).

Truncation of series in q depends strongly on the eccentricity (see e.g. Noyelles et al., 2014; Veras et al., 2019; Luna et al., 2020; Renaud et al., 2021). In our work, we will assume a fixed eccentricity, equal to its current value. Owing the low value of the lunar orbit eccentricity, it will be enough to take term up to $q_{\text{max}} = 10$, where q_{max} is the maximum value of $|q|$ in the sums over q (Luna et al., 2020). In other words, the sums over q extend from $q = -10$ up to $q = 10$. In general, $|q| \leq q_{\text{max}}$. In a future work, we will explore thermal and dynamical evolution considering different values of the eccentricity.

Another important issue concerning the values of the lunar orbital eccentricity (e) and inclination (i) with respect to the equatorial plane of the Earth must be addressed. For exploratory purposes, we have considered the current values for the two orbital parameters and assumed them to be fixed. Such an assumption could seem very simplistic, because all the parameters of the Moon's orbit evolve in time due to perturbations ranging from those of tidal origin to the gravitational attraction from other bodies, principally that of the Sun. In addition, grater values of both e and i can enhance tidal heating by activating modes corresponding to higher-than-synchronous spin-orbit resonances (Renaud et al., 2021). However, tidal heating is much more sensitive to variation of the eccentricity than of the inclination (Efroimsky & Makarov, 2014; Makarov & Efroimsky, 2014; Renaud et al., 2021). In this sense, we can expect that time evolution of the Moon's orbital inclination with respect to the Earth's equator has a negligible effect on the thermal evolution of our planet.

In what respects to the time evolution of the eccentricity, some recent works on the dynamical evolution of the Earth-Moon system that takes into account tidal evolution and solar perturbations (Ćuk & Stewart, 2012; Cuk et al., 2016; Wisdom & Tian, 2015; Tian et al., 2017, and references therein) obtain as result that lunar eccentricity varies between 0 and 0.1 or 0.2. In addition, the work by Rufu and Canup (2020) obtain higher eccentricities. However, it has to be pointed out that the aforementioned works make use of very simplistic rheological models, namely the Constant Phase Lag (CPL) (Wisdom & Tian, 2015; Tian et al., 2017) and the Constant Time

Lag (CTL) models (Rufu & Canup, 2020). These models do not describe appropriately the rheological response of a rocky planet or satellite (Efroimsky & Williams, 2009; Efroimsky, 2012; Efroimsky & Makarov, 2013). We would like to emphasize that the Darwin-Kaula expansion of the tidal disturbing potential from which Equation (32) for the rate of tidal heating (Efroimsky & Makarov, 2014) is derived, has the advantage of allowing the inclusion of any linear rheology as the ones considered in our work, such as the Maxwell-Andrade model which is a more realistic rheological model describing the response of a rocky material under stress (Efroimsky, 2012; Efroimsky, 2015; Renaud & Henning, 2018; Renaud et al., 2021). In addition, Maxwell-Andrade model has proven to be more dissipative than CPL and CTL ones (Renaud & Henning, 2018). Therefore, we can expect that numerical simulations using realistic rheologies could lead to a more enhanced eccentricity damping. Under the light of the aforementioned considerations, setting a constant value for the lunar eccentricity equal to its current value is a conservative assumption and the resulting rate of tidal heating and, consequently, the thermal evolution of the Earth's interior can be considered as a lower bound estimation.

In order to identify clearly the results obtained considering each regime, we will assign them a label and a number. The results obtained under the plate tectonics regime will be labeled with PT and the number 1 will be added when it is assumed that heat is only produced by the decay of radioactive isotopes, while the number 2 is included when tidal heating is allowed for, together with the considered rheological model. Analogously, in the stagnant lid regime, the corresponding results will be labeled with SL and a number with the same agreement as for the plate tectonics regime, i.e. when the label is followed by the number 1, only the radiogenic heat source is being considered. When the SL label is followed by number 2, radiogenic and tidal heat sources are taken into account, also indicating the particular rheological model. Each rheological model gives the functional form of the complex compliance, as is explained in the Supplementary information, and thus defines particular expressions of the complex Love numbers $K_{\mathrm{I}}(l, \omega_{lmpq})$ which in turn enter the expression for the tidal heating rate, i.e. Equation (32).

Thus, as an example, the results of the thermal evolution considered under the plate tectonics regime and assuming both tidal and radiogenic heat sources will be labeled with "PT2". Similarly, the results considering only the radiogenic heat source in the stagnant lid regime will be labeled with "SL1".

Regarding the initial conditions, we set the initial mean temperatures to be $\langle T\rangle_{\mathrm{c}}(0) = 5000\,\mathrm{K}$ and $\langle T\rangle_{\mathrm{m}}(0) = 2000\,\mathrm{K}$ for both the plate tectonics and the stagnant lid regimes. In addition, for the latter regime we set the initial lithosphere thickness $\ell(0) = 50\,\mathrm{km}$.

It is important to point out that the chosen values for the reference viscosity η_{ref} and temperature T_{ref} resulted in an excessive mantle's temperature increasing that equates that of the core's leading to a numerical collapse in our preliminary numerical experiments. In order to avoid this inconveniences we decided to change the value of the reference viscosity to $\eta_{\mathrm{ref}} = 4.5 \times 10^{24}\,\mathrm{Pa\,s}$. This practice is used to mimic the dependence of the viscosity on the pressure (see e.g. Walterová & Běhounková, 2020).

4 Results and discussion

We performed numerical simulations considering only the radiogenic heat source and then adding tidal heating for each of the three considered rheological models and for both the plate tectonics and stagnant lid regimes.

Figure 4 shows the evolution of the mean temperature over time for the Core and Mantle. As can be noted, Earth's core and mantle behave differently. Earth's

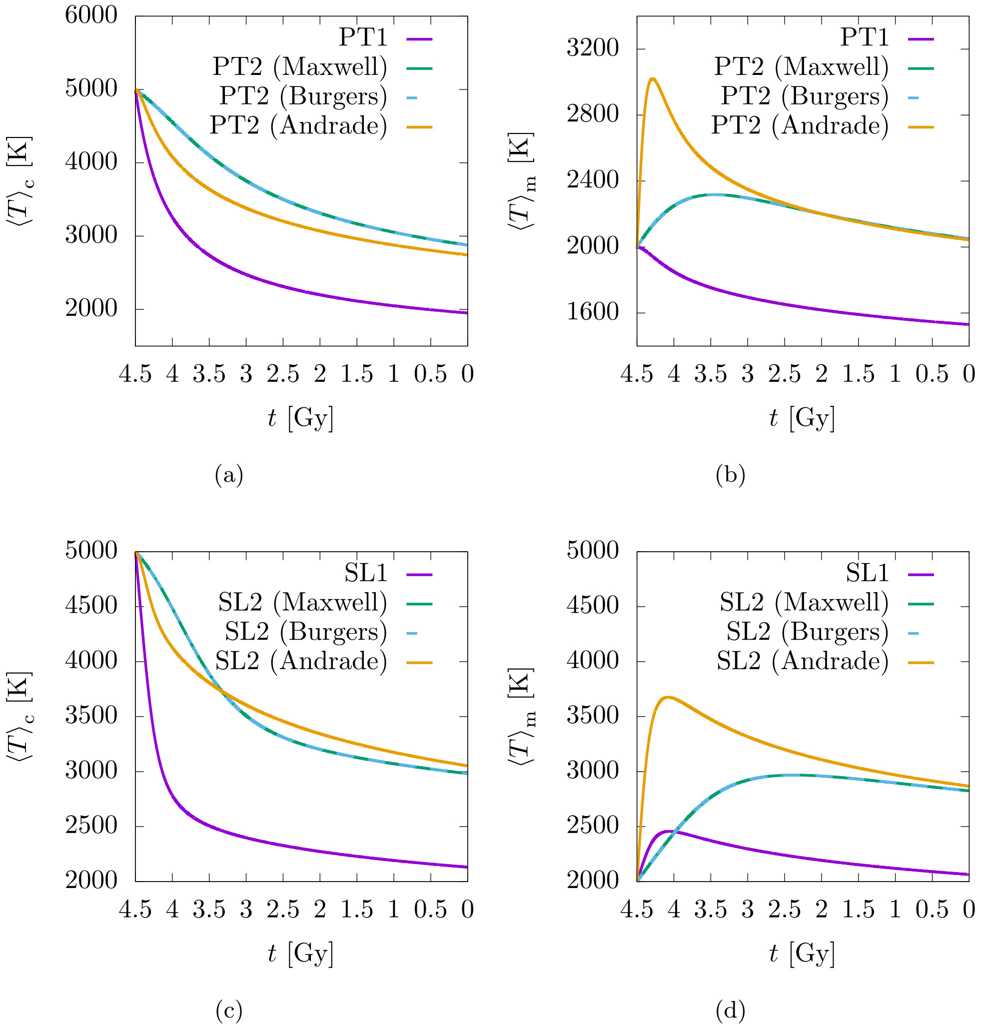

Figure 4: Thermal evolution of the Earth in the plate tectonics regime for the core (a) and mantle (b). Thermal evolution of the Earth in the stagnant lid regime for the core (c) and (d) mantle.

core temperature decreases in a exponentially-like fashion. However, the core cools down slower when tidal heating is taken into account (Figures 4a and 4c). Thermal evolution of the mantle is greatly affected by tidal heating. The shape of the curve in the evolution is appreciably changed. The impact of the tidal heating is stronger in the stagnant lid regime than in the plate tectonics one (see Figures 4b and 4d). When tidal heating is considered the mantle starts to cool down later than the case where tidal heating is neglected.

Considering that the major contribution of tidal heating is observed in the mantle (Henning & Hurford, 2014), we will focus our discussion on this layer. If we ignore the contribution of tidal heating, in the plate tectonics regime, mantle's temperature decreases uniformly from its initial value, as can be seen in Figure 4b, the corresponding line is the one labeled with PT1. However, if tidal heating is taken into account, then the thermal evolution of the mantle differs significantly. Using the Maxwell and Burgers rheological models, $\langle T \rangle_{\mathrm{m}}$ increases over the first billion of years of evolution,

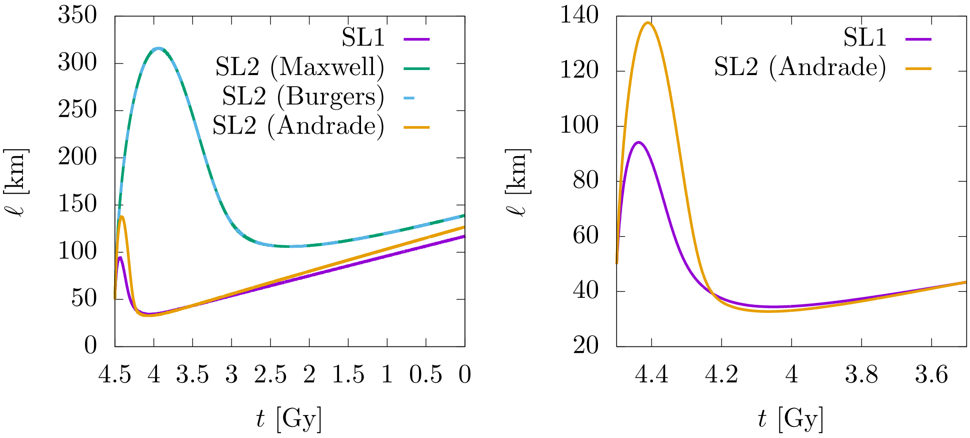

(a) (b)

Figure 5: (a) Time evolution of the lithosphere thickness over the Earth's history. (b) Comparison between numerical experiments SL1 and SL2, using the Maxwell-Andrade rheology, over the time interval from 4.5 to 3.5 Gy in the past.

then the temperature starts decreasing. It has to be pointed out that the corresponding lines of the aforementioned models are overlapped. A more realistic rheology, such as the Maxwell-Andrade one, results in a temperature overshoot in the first 0.5 Gy before the temperature begin to decrease.

Contrary to plate tectonics regime, in the stagnant lid regime the thermal evolution shows an increasing of temperature in the first billion of years of evolution either with or without taking into account tidal dissipation. Nevertheless the increment in temperature without tidal dissipation is lower reaching only 2500 K, as is shown in Figure 4d by the curve labeled with SL1.

Both the Maxwell and the Burgers rheological models give the same thermal evolution for the mantle and for each thermal regime. In the plate tectonics regime, mantle's temperature begins to decrease after 1 Gy for the Maxwell and Burgers models, and after approximately 0.25 Gy for the Maxwell-Andrade model. In the stagnant lid regime, mantle begins to cool down somewhat later. For the Maxwell and Burgers model mantle's temperature starts decreasing after 2 Gy, and for the Maxwell-Andrade models it begins cooling after 0.5 Gy. Again, we observe a temperature overshooting of about 1600 K in the first 0.5 Gy in the mantle temperature when the Maxwell-Andrade model is considered in the SL regime.

Such temperature increasing could result in partial melting of at least some of the materials composing the primordial Earth's mantle. As we have pointed out when presenting the thermal models (Section 2), these do not take into account phase transitions. However, for this exploratory work, we are considering only the time evolution of the average mantle temperature. This means that there could be partial melting locally in some regions of the mantle, but in no way such temperature increasing or overshooting means that the mantle is totally melt.

Concerning the time evolution of the lithosphere thickness, we observe in Figure 5a that for all the cases ℓ increases rapidly in the very first 0.5 Gy and then decreases up to a minimum and then starts increasing again but at a lower rate. It is interesting

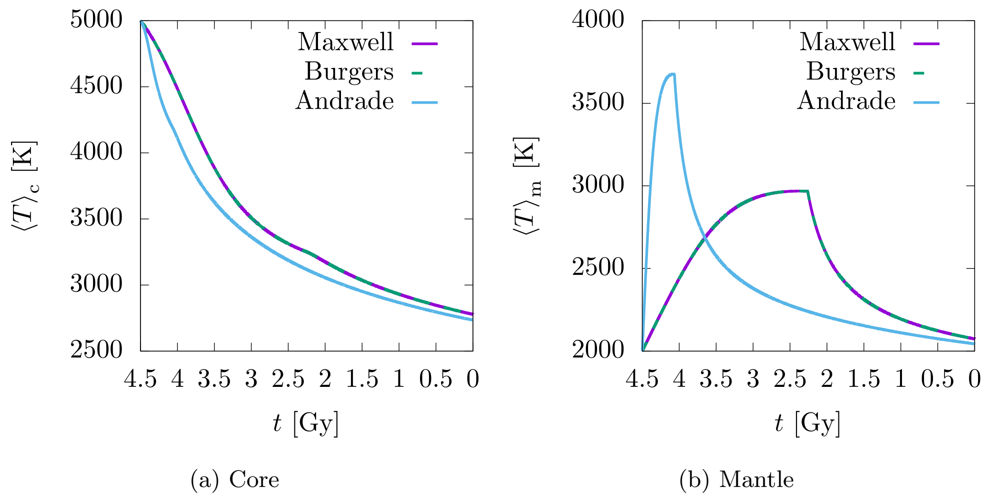

Figure 6: (a) Thermal evolution of the Earth's core and (b) mantle as result from the combined thermal regime model, exploring the Maxwell, Burgers and Maxwell-Andrade rheological models.

to note that when tidal heating is ignored (SL1 curve) and when it is considered, for the Maxwell-Andrade model, at least for the set of parameters explored, nearly the same minimum is obtained after the first 500 My of evolution, where the lithosphere thickness is less than 50 km. However, a somewhat thinner lithosphere is obtained considering tidal heating with the Maxwell-Andrade model, as can be observed in Figure 5b.

In our model of plate tectonics we cannot evaluate the evolution of lithosphere due to the inclusion of this layer in the global convection of the mantle. Yet, we can study the impact of the onset of plate tectonics on the thermal evolution of the Earth's interior. To this end, we propose a "combined" thermal model to describe the transition from the stagnant lid regime to the plate tectonics one. We assume that the aforementioned regime transition occurs when the curve describing the time evolution of the lithosphere thickness reaches a local minimum (Figure 5). In this sense, the change from one regime to the other is forced in the considered model. Although this is an arbitrary criterion, it corresponds to an "educated guess" because we expect that a thin lithosphere yields to a more favorable scenario for the plate subduction and, consequently, the onset of plate tectonics.

We performed three numerical simulations, taking in account the tidal heating and using the same initial conditions for the core's and mantle's temperatures and lithosphere thickness, exploring the three rheological models proposed. The results are shown in Figure 6a and 6b. The former depicts the time evolution of the mean core temperature, while the latter shows the time evolution of the mean mantle temperature.

In total correspondence with Figure 5, it can be seen in Figure 6b that the Maxwell-Andrade model leads to a regime transition about 2 Gy earlier than Maxwell and Burgers models. The regime transition occurs after the first 0.5 Gy of evolution when the Maxwell-Andrade model is considered. The Maxwell and Burgers models predict a regime transition between 2 and 2.5 Gy in the past.

Maxwell-Andrade model also produces a temperature overshoot, as in the previous results, which is rapidly damped, as well as the temperature increase produced by the Maxwell and Burgers models, showing the high efficiency of convection in the plate tectonics regime to remove heat from the mantle. In Figure 6a we can observe that thermal evolution of the core reflects that of the mantle. Figure 6b shows that using the Burgers or Maxwell rheologies the Mantle cooling delays until 2 Ma while the Andrade rheology predicts a minimum lithosphere and mantle cooling as early as 4 Gy ago.

In Section 3.1 we considered a dynamical evolution model (DEM) which describes the time evolution of the major semiaxis of the Moon's orbit and the length of Earth's day. That model was obtained by fitting the geological data to a cubic polynomial. However, we may now wonder how would be affected the thermal history of the Earth if the Moon recess and the Earth spins down in different ways. In order to answer that question, we proposed two different linear models for the dynamical evolution. We identify the three models by the label DEM and an ID number. Thus, DEM1 correspond to the cubic polynomials fitting the geological data. DEM2 is obtained by assuming both that the Moon is spiraling outwards at a constant rate equal to the current value of the time derivative of the major semiaxis with respect to time, obtained by LLR, i.e., $(\mathrm{d}a/\mathrm{d}t)_0 = 3.82 \times 10^{-2}\,\mathrm{m\,yr^{-1}}$ (Bills & Ray, 1999) and that the LOD increases linearly from its estimated initial value of 6.15 hours (4.5 Gy ago) to its current value of 23.93 hours. It worth to point out that the latter DEM implies an initial value for the major semiaxis of about $2.125 \times 10^8\,\mathrm{m}$. Finally, DEM3 also correspond to constant recession of the Moon from an arbitrary value of $20\,R_\oplus$ to its present value (Table S2), while LOD increases linearly from only 2.53 hours to its current value (Tian et al., 2017). In Figures S3 and S4 of the Supplementary information we plot the assumed time evolution of the major semiaxis of the lunar orbit and the Earth's LOD, respectively.

We evaluated these three evolution models of Moon's major semiaxis and Earth's rotation period and how they impacted in Earth interior temperature applying the combined model which considers the stagnant lid regime until a minimum value of ℓ is reached and then continues the integration considering the plate tectonics regime. The results are shown in Figure 7. As can be noticed in Panels (a), (b), (d) and (e) of Figure 7, we find that there is no difference between the thermal histories of the Earth's core and mantle when the Maxwell and Burgers rheological models are considered. However, it is very interesting how relevant can be the influence of the dynamical history of the Earth-Moon system on the thermal evolution of the Earth's interior when the Maxwell-Andrade model is used to model the rheology of the mantle. As it is shown in Figure 7c and 7f three different thermal evolution are obtained, each corresponding to a particular DEM.

The curve corresponding to DEM1 in Figure 7f, describes the same thermal history of the mantle as that of Figure 6b. Both figures show a mean temperature overshoot of about 1700 K over its initial value and then start decreasing rapidly due to the change from the stagnant lid regime to the plate tectonics one. This reflects the fact that DEM1 is characterized by a swift increase of the mean distance between Earth and Moon. If our natural satellite moves away more slowly, as prescribed by DEM2, we obtain a somewhat higher temperature overshoot that becomes damped later that the latter case. As expected, if the Moon was farther away at the beginning of the dynamical history of the system it forms with Earth, and receding at a constant rate equal to the current value, then the mean mantle temperature increases up to 3000 K and the regime transition takes place about 2 Gy later than the aforementioned cases.

It worth to point out that geological evidences support the hypothesis of an initially fast rotating Earth. In addition, several theories were capable to reproduce the current dynamical state of the Earth-Moon system assuming the formation of the

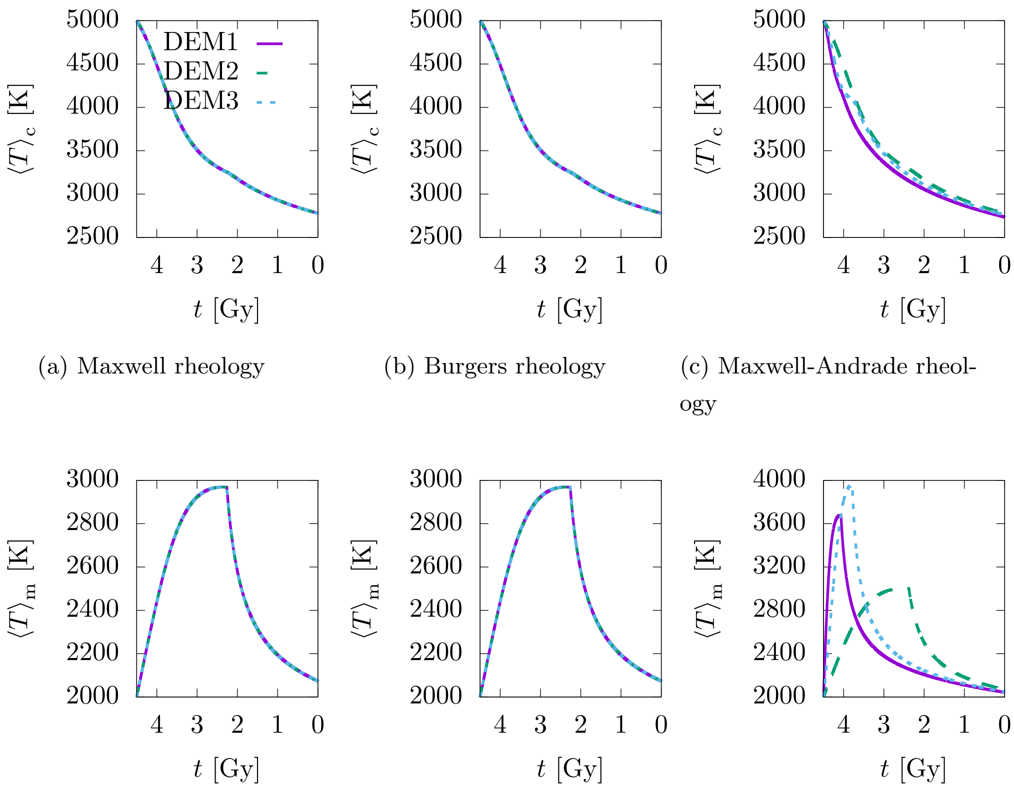

(a) Maxwell rheology (b) Burgers rheology (c) Maxwell-Andrade rheology

(d) Maxwell rheology (e) Burgers rheology (f) Maxwell-Andrade rheology

Figure 7: Thermal evolution of the Earth's core –(a), (b) and (c)– and mantle –(d), (e) and (f)– as result of the numerical experiments performed considering three different dynamical evolution models (DEM1, DEM2 and DEM3), for the three rheological models considered in our work.

Moon from a giant impact (Hartmann & Davis, 1975; Cameron & Ward, 1976; Canup, 2004, 2008).

However, the so-called "canonicaĺ" theory has two main difficulties. On one hand, it can not explain satisfactorily the isotopic similarities between Earth and Moon (Lugmair & Shukolyukov, 1998; Wiechert et al., 2001; Touboul et al., 2007; Meier, 2012; Zhang et al., 2012; Young et al., 2016). On the other hand, that theory, which is based on numerical simulations of the Moon-forming giant impact, assumes the conservation of the total angular momentum of the Earth-Moon system along its whole history.

In order to reconcile the giant impact theory with isotopic similarities between the Earth and Moon, alternative models have been proposed (Pahlevan & Stevenson, 2007; Ćuk & Stewart, 2012; Canup, 2012; Reufer et al., 2012). In particular, the works by Canup (2012) and Ćuk and Stewart (2012) propose that the aforementioned difficulties may be overcome by loosening the angular momentum conservation constraint assuming a rapidly rotating Earth after the impact. The results of the numerical simulations performed under the latter assumption not only agrees with the geologi-

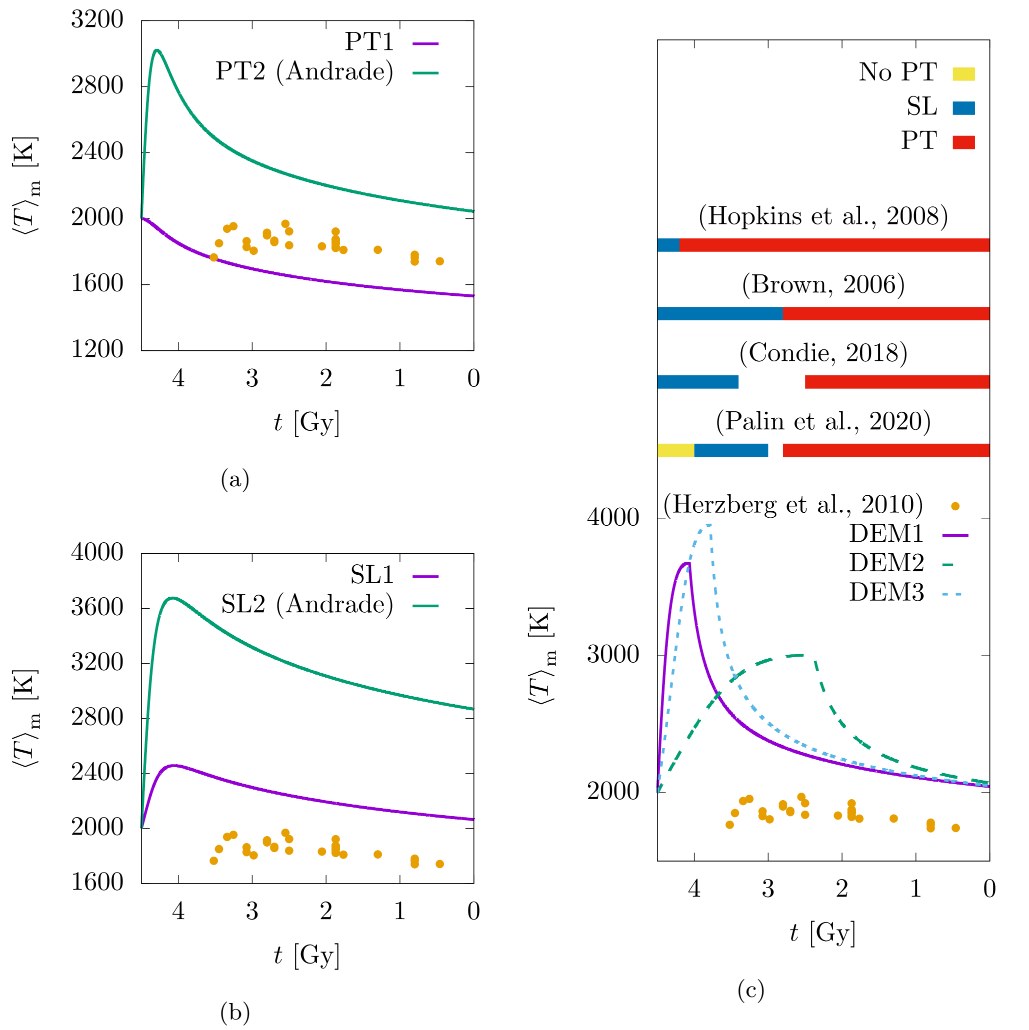

Figure 8: Comparative plots between the results obtained from our numerical simulations, under the plate tectonics (a), stagnant lid (b) and the combined model (c), and the results from the work by Herzberg et al. (2010).

cal data, but also agree with the empirical fact that the Moon is formed mainly by mantle-derived materials.

5 Conclusions

In this work, we explored the influence of tidal heating on the thermal evolution of Earth's interior. To this end, we investigate two end members of thermal model regimes, namely plate tectonics and stagnant lid regimes. Moreover, for each of those scenarios we evaluate different rheological models for the Earth's mantle. For these models we have considered the decay of the most thermally relevant radioactive isotopes and tidal heat sources.

As result of the numerical simulations carried out, we obtained that tidal heating could have played a relevant role in the thermal history of the Earth in the first billions of years. In addition, the study of the time evolution of the lithosphere thickness opens the possibility of studying the consequence of tidal heating on the onset of plate tectonics.

The importance of the rheological model applied for modeling should be emphasized. In this sense, the influence of tidal heating is not trivial and its relevance for the Earth's thermal evolution depends on the model used. Moreover, our results show that it becomes crucial to know the evolution of the Moon's orbit and Earth's rotation properly, to be able to model the terrestrial thermal evolution.

Taking into account that the closer the Moon to the Earth the more tidal heat it brings to the latter, we conclude that the orbital evolution controls not only the magnitude of tidal heating but also the rate at which mantle cools down. Throughout our numerical experiments we have demonstrated that the steeper the slope of the recession rate the greater the temperature loss.

After our analysis, it is interesting to compare the results with geological evidences on the onset of plate tectonics and terrestrial geodynamics. In this sense, we compared our results with the data from the work of Herzberg et al. (2010) for mantle temperature at different periods of Earth history.

As shown in Figure 8a the mantle temperature data are higher than our plate tectonic model without tidal heating, and at the same time lower but close to the plate tectonic model taking into account tidal heating. This is interesting since the data from the work by Herzberg et al. (2010) represent the upper mantle (shallower than 300 km depth), while our model represents the average mantle temperature. Thus, the fact that the data are above the TP1 curve suggest that an extra heat source is needed to reproduce those data since the mean mantle temperature must always be higher than that of its outermost regions. The TP2 curve laying above the data suggests that tidal heating input could have been necessary in the Earth's history. In Figure 8b it is observed that, on one hand, thermal models considering the stagnant regime describe a higher mantle temperature since the SL1 and SL2 model curves are above the data. However, a stagnant lid regime over the entire Earth's history is infeasible. On the other hand, tidal heat would not be needed in the stagnant lid regime. In addition, thermal model considering the stagnant lid regime including tidal heating would have generated a temperature rise in the early Gy and a slow decline (O'Neill, 2020) obtaining a similar pattern reminiscent of the data.

In the previous section, we analyzed different dynamical evolution models (DEMs) of the Earth-Moon system, concluding that according to the model used, the recession rate of the Moon has a significant influence on the thermal evolution of the mantle (Figure 7f). Comparing these results with the different estimations for the origin of plate tectonics, (Figure 8c) we observe that our models coincide with the time window that different authors propose for the onset of plate tectonics (Brown, 2006; Hopkins et al., 2008; Condie, 2018; Palin et al., 2020). In addition, we also conclude that since the thermal evolution of the mantle strongly depends on the dynamical evolution model, it may be interesting to use geological evidence and thermal models to constrain the dynamical evolution of the Earth-Moon system.

According to our models, the minimum of lithospheric thickness is reached within the proposed time window for the onset of plate tectonics. As Korenaga (2013) points out, in the past the buoyancy of the lithosphere would have been greater due to greater thickness, preventing plate tectonics scenario. Before this time our models also predict a greater thickness which would lead to greater buoyancy and inhibition of subduction, as was also proposed by some authors (Korenaga, 2013, and reference therein).

Taking into account different models of dynamical evolution to evaluate the temperature of the mantle, we conclude that the thermal trend of the Earth become spiky, with larger amplitudes when the tidal heating is considered (Figures 4 and 5). This extra heat could have had some impact in the large geologic and geochemical changes that would have occurred between 2 and 3 Gy ago (Condie, 2018; Palin et al., 2020). This leads us to propose for a future work that using geological and petrological evidence of the temperature of the Earth's mantle could give clues to lunar orbital evolution and Earth's rotational evolution by using this type of models backwards.

Our work shows that tidal heating could have played a predominant role in the early stages of terrestrial evolution and should be considered in thermal modeling. However, the magnitude by which it would have been affected is highly dependent on the rheological model used. We conclude that our results can contribute to the understanding of the Earth's dynamics in the hadean/archean and should be taken into account when studying the origin of plate tectonics on Earth.

Acknowledgments

S. H. Luna and M. G. Spagnuolo acknowledge funding from the Consejo Nacional de Investigaciones Científicas y Técnicas (CONICET) through PUE 22920160100051. S. H. Luna and H. D. Navone acknowledge funding from Universidad Nacional de Rosario through PID ING 545. Data for reproducing the time evolution of Earth's LOD and lunar major simaxis is available through López de Azarevich and Azarevich (2017), Williams (2000), and Spalding and Fischer (2019). Data of the mantle temperature through time shown in Figure 8 is available through Herzberg et al. (2010).

References

Bills, B. G., & Ray, R. D. (1999). Lunar orbital evolution: A synthesis of recent results. *Geophysical Research Letters*, *26*(19), 3045-3048. Retrieved from `https://agupubs.onlinelibrary.wiley.com/doi/abs/10.1029/1999GL008348` doi: https://doi.org/10.1029/1999GL008348

Brown, M. (2006, 11). Duality of thermal regimes is the distinctive characteristic of plate tectonics since the Neoarchean. *Geology*, *34*(11), 961-964. Retrieved from `https://doi.org/10.1130/G22853A.1` doi: 10.1130/G22853A.1

Cameron, A. G. W., & Ward, W. R. (1976). The origin of the moon. In Lunar & P. Institute (Eds.), *Proceedings of the seventh lunar science conference.* Retrieved from `https://www.lpi.usra.edu/meetings/lsc1976/pdf/1041.pdf`

Canup, R. M. (2004). Simulations of a late lunar-forming impact. *Icarus*, *168*(2), 433 - 456. Retrieved from `http://www.sciencedirect.com/science/article/pii/S0019103503002999` doi: https://doi.org/10.1016/j.icarus.2003.09.028

Canup, R. M. (2008). Lunar-forming collisions with pre-impact rotation. *Icarus*, *196*(2), 518-538. Retrieved from `https://www.sciencedirect.com/science/article/pii/S0019103508001280` (Mars Polar Science IV) doi: https://doi.org/10.1016/j.icarus.2008.03.011

Canup, R. M. (2012). Forming a moon with an earth-like composition via a giant impact. *Science*, *338*(6110), 1052–1055. Retrieved from `https://science.sciencemag.org/content/338/6110/1052` doi: 10.1126/science.1226073

Carslaw, H. S., & Jaeger, J. C. (1959). *Conduction of heat in solids.* Oxford Science publications.

Castillo-Rogez, J. C., Efroimsky, M., & Lainey, V. (2011). The tidal history of iapetus: Spin dynamics in the light of a refined dissipation model. *Journal of Geophysical Research: Planets*, *116*(E9), n/a–n/a. Retrieved from `http://dx.doi.org/10.1029/2010JE003664` (E09008) doi: 10.1029/2010JE003664

Condie, K. C. (2018). A planet in transition: The onset of plate tectonics on earth between 3 and 2 ga? *Geoscience Frontiers*, *9*(1), 51 - 60. Retrieved from http://www.sciencedirect.com/science/article/pii/S167498711630127X (Lid Tectonics) doi: https://doi.org/10.1016/j.gsf.2016.09.001

Cuk, M., Hamilton, D., Lock, S., & Stewart, S. (2016). Tidal evolution of the moon from a high-obliquity, high-angular-momentum earth. *Nature*, *539*, 402-406.

Ćuk, M., & Stewart, S. T. (2012). Making the moon from a fast-spinning earth: A giant impact followed by resonant despinning. *Science*, *338*(6110), 1047–1052. Retrieved from https://science.sciencemag.org/content/338/6110/1047 doi: 10.1126/science.1225542

Efroimsky, M. (2012, March). Bodily tides near spin-orbit resonances. *Celestial Mechanics and Dynamical Astronomy*, *112*, 283-330. doi: 10.1007/s10569-011-9397-4

Efroimsky, M. (2015, sep). Tidal Evolution of Asteroidal Binaries. Ruled by Viscosity. Ignorant of Rigidity. *The Astronomical Journal*, *150*(4), 98. Retrieved from https://doi.org/10.1088%2F0004-6256%2F150%2F4%2F98 doi: 10.1088/0004-6256/150/4/98

Efroimsky, M., & Makarov, V. V. (2013, jan). Tidal friction and tidal lagging. Applicability limitations of a popular formula for the tidal torque. *The Astrophysical Journal*, *764*(1), 26. Retrieved from https://doi.org/10.1088/0004-637x/764/1/26 doi: 10.1088/0004-637x/764/1/26

Efroimsky, M., & Makarov, V. V. (2014, oct). Tidal dissipation in a homogeneous spherical body. i. Methods. *The Astrophysical Journal*, *795*(1), 6. Retrieved from https://doi.org/10.1088%2F0004-637x%2F795%2F1%2F6 doi: 10.1088/0004-637x/795/1/6

Efroimsky, M., & Williams, J. G. (2009, July). Tidal torques: a critical review of some techniques. *Celestial Mechanics and Dynamical Astronomy*, *104*, 257-289. doi: 10.1007/s10569-009-9204-7

Giacaglia, G. E. O. (1976, December). A note on Hansen's coefficients in satellite theory. *Celestial Mechanics*, *14*, 515-523. doi: 10.1007/BF01229062

Gooding, R. H., & Wagner, C. A. (2008, July). On the inclination functions and a rapid stable procedure for their evaluation together with derivatives. *Celestial Mechanics and Dynamical Astronomy*, *101*, 247-272. doi: 10.1007/s10569-008-9145-6

Grott, M., & Breuer, D. (2008). The evolution of the martian elastic lithosphere and implications for crustal and mantle rheology. *Icarus*, *193*(2), 503 - 515. Retrieved from http://www.sciencedirect.com/science/article/pii/S001910350700365X (Saturn's Icy Satellites from Cassini) doi: https://doi.org/10.1016/j.icarus.2007.08.015

Hartmann, W. K., & Davis, D. R. (1975). Satellite-sized planetesimals and lunar origin. *Icarus*, *24*(4), 504-515. Retrieved from https://www.sciencedirect.com/science/article/pii/0019103575900706 doi: https://doi.org/10.1016/0019-1035(75)90070-6

Henning, W. G., & Hurford, T. (2014, jun). TIDAL HEATING IN MULTILAYERED TERRESTRIAL EXOPLANETS. *The Astrophysical Journal*, *789*(1), 30. Retrieved from https://doi.org/10.1088%2F0004-637x%2F789%2F1%2F30 doi: 10.1088/0004-637x/789/1/30

Henning, W. G., O'Connell, R. J., & Sasselov, D. D. (2009, dec). TIDALLY HEATED TERRESTRIAL EXOPLANETS: VISCOELASTIC RESPONSE MODELS. *The Astrophysical Journal*, *707*(2), 1000–1015. Retrieved from https://doi.org/10.1088%2F0004-637x%2F707%2F2%2F1000 doi: 10.1088/0004-637x/707/2/1000

Herzberg, C., Condie, K., & Korenaga, J. (2010). Thermal history of the earth and its petrological expression. *Earth and Planetary Science Letters*, *292*(1), 79-88. Retrieved from https://www.sciencedirect.com/science/article/pii/S0012821X10000567 doi: https://doi.org/10.1016/j.epsl.2010.01.022

Hopkins, M., Harrison, T. M., & Manning, C. E. (2008, Nov 01). Low heat flow inferred from ¿4 gyr zircons suggests hadean plate boundary interactions. *Nature*, *456*(7221), 493-496. Retrieved from https://doi.org/10.1038/nature07465 doi: 10.1038/nature07465

Karato, S., & Spetzler, H. A. (1990, November). Defect microdynamics in minerals and solid state mechanisms of seismic wave attenuation and velocity dispersion in the mantle. *Reviews of Geophysics*, *28*, 399-421. doi: 10.1029/RG028i004p00399

Korenaga, J. (2013). Initiation and evolution of plate tectonics on earth: Theories and observations. *Annual Review of Earth and Planetary Sciences*, *41*(1), 117-151. Retrieved from https://doi.org/10.1146/annurev-earth-050212-124208 doi: 10.1146/annurev-earth-050212-124208

Lugmair, G., & Shukolyukov, A. (1998). Early solar system timescales according to 53mn-53cr systematics. *Geochimica et Cosmochimica Acta*, *62*(16), 2863-2886. Retrieved from https://www.sciencedirect.com/science/article/pii/S0016703798001896 doi: https://doi.org/10.1016/S0016-7037(98)00189-6

Luna, S. H., Navone, H. D., & Melita, M. D. (2020). The dynamical evolution of close-in binary systems formed by a super-earth and its host star - case of the kepler-21 system. *A&A*, *641*, A109. Retrieved from https://doi.org/10.1051/0004-6361/201936551 doi: 10.1051/0004-6361/201936551

López de Azarevich, V. L., & Azarevich, M. B. (2017). Lunar recession encoded in tidal rhythmites: a selective overview with examples from argentina. *Geo-Marine Letters*, *37*(4), 333-344. Retrieved from https://doi.org/10.1007/s00367-017-0500-z doi: 10.1007/s00367-017-0500-z

Makarov, V. V. (2013, 06). Why is the Moon synchronously rotating? *Monthly Notices of the Royal Astronomical Society: Letters*, *434*(1), L21-L25. Retrieved from https://doi.org/10.1093/mnrasl/slt068 doi: 10.1093/mnrasl/slt068

Makarov, V. V., & Efroimsky, M. (2014, Nov). Tidal Dissipation in a Homogeneous Spherical Body. II. Three Examples: Mercury, IO, and Kepler-10 b. *Astrophysical Journal*, *795*(1), 7. doi: 10.1088/0004-637X/795/1/7

Meier, M. M. M. (2012, Apr 01). Earth's titanium twin. *Nature Geoscience*, *5*(4), 240-241. Retrieved from https://doi.org/10.1038/ngeo1434 doi: 10.1038/ngeo1434

Murray, C. D., & Dermott, S. F. (1999). *Solar system dynamics.* Cambridge University Press.

Noyelles, B., Frouard, J., Makarov, V. V., & Efroimsky, M. (2014). Spin-orbit evolution of mercury revisited. *Icarus*, *241*, 26 - 44. Retrieved from http://www.sciencedirect.com/science/article/pii/S0019103514003078 doi: https://doi.org/10.1016/j.icarus.2014.05.045

O'Neill, C. (2020). Planetary thermal evolution models with tectonic transitions. *Planetary and Space Science*, *192*, 105059. Retrieved from https://www.sciencedirect.com/science/article/pii/S0032063320302725 doi: https://doi.org/10.1016/j.pss.2020.105059

Pahlevan, K., & Stevenson, D. J. (2007). Equilibration in the aftermath of the lunar-forming giant impact. *Earth and Planetary Science Letters*, *262*(3), 438-449. Retrieved from https://www.sciencedirect.com/science/article/pii/S0012821X07005006 doi: https://doi.org/10.1016/j.epsl.2007.07.055

Palin, R. M., Santosh, M., Cao, W., Li, S.-S., Hernández-Uribe, D., & Parsons, A. (2020). Secular change and the onset of plate tectonics on earth. *Earth-Science Reviews*, *207*, 103172. Retrieved from https://www.sciencedirect.com/science/article/pii/S001282522030218X doi: https://doi.org/10.1016/j.earscirev.2020.103172

Renaud, J. P., & Henning, W. G. (2018, apr). Increased tidal dissipation using advanced rheological models: Implications for io and tidally active exoplanets.

The Astrophysical Journal, *857*(2), 98. Retrieved from https://doi.org/10.3847/1538-4357/aab784 doi: 10.3847/1538-4357/aab784

Renaud, J. P., Henning, W. G., Saxena, P., Neveu, M., Bagheri, A., Mandell, A., & Hurford, T. (2021, jan). Tidal dissipation in dual-body, highly eccentric, and nonsynchronously rotating systems: Applications to pluto–charon and the exoplanet TRAPPIST-1e. *The Planetary Science Journal*, *2*(1), 4. Retrieved from https://doi.org/10.3847/psj/abc0f3 doi: 10.3847/psj/abc0f3

Reufer, A., Meier, M. M., Benz, W., & Wieler, R. (2012). A hit-and-run giant impact scenario. *Icarus*, *221*(1), 296-299. Retrieved from https://www.sciencedirect.com/science/article/pii/S0019103512002977 doi: https://doi.org/10.1016/j.icarus.2012.07.021

Rufu, R., & Canup, R. M. (2020). Tidal evolution of the evection resonance/quasi-resonance and the angular momentum of the earth-moon system. *Journal of Geophysical Research: Planets*, *125*(8), e2019JE006312. Retrieved from https://agupubs.onlinelibrary.wiley.com/doi/abs/10.1029/2019JE006312 (e2019JE006312 10.1029/2019JE006312) doi: https://doi.org/10.1029/2019JE006312

Schubert, G., Cassen, P., & Young, R. (1979). Subsolidus convective cooling histories of terrestrial planets. *Icarus*, *38*(2), 192 - 211. Retrieved from http://www.sciencedirect.com/science/article/pii/0019103579901787 doi: https://doi.org/10.1016/0019-1035(79)90178-7

Spalding, C., & Fischer, W. W. (2019). A shorter archean day-length biases interpretations of the early earth's climate. *Earth and Planetary Science Letters*, *514*, 28 - 36. Retrieved from http://www.sciencedirect.com/science/article/pii/S0012821X19301359 doi: https://doi.org/10.1016/j.epsl.2019.02.032

Spohn, T. (1991). Mantle differentiation and thermal evolution of mars, mercury, and venus. *Icarus*, *90*(2), 222 - 236. Retrieved from http://www.sciencedirect.com/science/article/pii/001910359190103Z doi: https://doi.org/10.1016/0019-1035(91)90103-Z

Stacey, F. D., & Davis, P. M. (2008). *Physics of the earth* (Fourth ed.). Cambridge University Press.

Stamenković, V., Noack, L., Breuer, D., & Spohn, T. (2012, mar). THE INFLUENCE OF PRESSURE-DEPENDENT VISCOSITY ON THE THERMAL EVOLUTION OF SUPER-EARTHS. *The Astrophysical Journal*, *748*(1), 41. Retrieved from https://doi.org/10.1088%2F0004-637x%2F748%2F1%2F41 doi: 10.1088/0004-637x/748/1/41

Tian, Z., Wisdom, J., & Elkins-Tanton, L. (2017). Coupled orbital-thermal evolution of the early earth-moon system with a fast-spinning earth. *Icarus*, *281*, 90-102. Retrieved from https://www.sciencedirect.com/science/article/pii/S0019103516302780 doi: https://doi.org/10.1016/j.icarus.2016.08.030

Touboul, M., Kleine, T., Bourdon, B., Palme, H., & Wieler, R. (2007, Dec 01). Late formation and prolonged differentiation of the moon inferred from w isotopes in lunar metals. *Nature*, *450*(7173), 1206-1209. Retrieved from https://doi.org/10.1038/nature06428 doi: 10.1038/nature06428

Turcotte, D., & Schubert, G. (2014). *Geodynamics* (3rd ed.). Cambridge University Press.

Valencia, D., O'Connell, R. J., & Sasselov, D. (2006, Apr). Internal structure of massive terrestrial planets. *Icarus*, *181*(2), 545-554. doi: 10.1016/j.icarus.2005.11.021

Veras, D., Efroimsky, M., Makarov, V. V., Boué, G., Wolthoff, V., Reffert, S., ... Gänsicke, B. T. (2019, 05). Orbital relaxation and excitation of planets tidally interacting with white dwarfs. *Monthly Notices of the Royal Astronomical Society*, *486*(3), 3831-3848. Retrieved from https://doi.org/10.1093/mnras/stz965 doi: 10.1093/mnras/stz965

Walterová, M., & Běhounková, M. (2020, aug). Thermal and orbital evolution of low-mass exoplanets. *The Astrophysical Journal*, *900*(1), 24. Retrieved from `https://doi.org/10.3847/1538-4357/aba8a5` doi: 10.3847/1538-4357/aba8a5

Wiechert, U., Halliday, A. N., Lee, D.-C., Snyder, G. A., Taylor, L. A., & Rumble, D. (2001). Oxygen isotopes and the moon-forming giant impact. *Science*, *294*, 345-348.

Williams, G. E. (2000). Geological constraints on the precambrian history of earth's rotation and the moon's orbit. *Reviews of Geophysics*, *38*(1), 37-59. Retrieved from `https://agupubs.onlinelibrary.wiley.com/doi/abs/10.1029/1999RG900016` doi: 10.1029/1999RG900016

Wisdom, J., & Tian, Z. (2015). Early evolution of the earth–moon system with a fast-spinning earth. *Icarus*, *256*, 138-146. Retrieved from `https://www.sciencedirect.com/science/article/pii/S0019103515000779` doi: https://doi.org/10.1016/j.icarus.2015.02.025

Young, E. D., Kohl, I. E., Warren, P. H., Rubie, D. C., Jacobson, S. A., & Morbidelli, A. (2016). Oxygen isotopic evidence for vigorous mixing during the moon-forming giant impact. *Science*, *351*(6272), 493–496. Retrieved from `https://science.sciencemag.org/content/351/6272/493` doi: 10.1126/science.aad0525

Zhang, J., Dauphas, N., Davis, A. M., Leya, I., & Fedkin, A. (2012, Apr 01). The proto-earth as a significant source of lunar material. *Nature Geoscience*, *5*(4), 251-255. Retrieved from `https://doi.org/10.1038/ngeo1429` doi: 10.1038/ngeo1429

Supporting Information for "The influence of tidal heating on the Earth's thermal evolution along the dynamical history of the Earth-Moon system"

S. H. Luna[1], M. G. Spagnuolo[2], H. D. Navone[3,4]

[1]Instituto de Estudios Andinos "Don Pablo Groeber" (IDEAN). Universidad de Buenos Aires – CONICET. Intendente Güiraldes 2160, Ciudad Universitaria, Pabellón II, C1428EGA, Ciudad Autónoma de Buenos Aires, Argentina.

[2]Instituto de Estudios Andinos "Don Pablo Groeber" (IDEAN). Universidad de Buenos Aires – CONICET. Intendente Güiraldes 2160, Ciudad Universitaria, Pabellón II, C1428EGA, Ciudad Autónoma de Buenos Aires, Argentina. E-mail: mgspag@gmail.com

[3]Facultad de Ciencias Exactas, Ingeniería y Agrimensura. Universidad Nacional de Rosario. Av. Pellegrini 250, S2000BTP, Rosario, Argentina.

[4]Instituto de Física de Rosario (IFIR). CONICET – Universidad Nacional de Rosario. Bv. 27 de Febrero, S2000EKF, Rosario, Argentina.

Contents of this file

Introduction

In this document we present the derivation of the general expression for the heat flux through a conductive lid in a setting where heat transport is dominated by convection, together with the corresponding figures. In addition, we reproduce the expression of $H(t)$, i.e. the rate at which heat is produced by decay of radioactive elements, and the functional form of the quality factors $K_{\mathrm{I}}\left(l, \chi_{lmpq}\right)$ present in the expression of the tidal heating rate. Tables S1, necessary for the computation of $H(t)$, Tables S2 and S3 are also included for the implementation of the numerical models.

Text S1. Derivation of the convecting heat flux expressions

The dominant heat transfer mechanism inside Earth is convection on geological time scales. In our work, we will make use of the *boundary layer approach* (Turcotte & Schubert, 2014) in order to obtain simple expressions of the heat flow in the convection regime. Briefly speaking, under specific circumstances, the temperature profile of a fluid in the thermal convection regime, flowing over or below a heated or cooled surface, can described as a temperature profile corresponding to thermal conduction through a thin lid followed by an isothermal profile (see Figure S2).

The Nusselt number is defined as the ratio of heat flux transported by convection to that by conduction (Turcotte & Schubert, 2014). Mathematically expressed:

$$\mathrm{Nu} = \frac{q^{\mathrm{conv}}}{q^{\mathrm{cond}}} \tag{S-1}$$

By virtue of what we have pointed out before, we then have that $\mathrm{Nu} \gg 1$. Another useful definition of the Nusselt number, that fits the purposes of our work, is the following (Turcotte & Schubert, 2014):

$$\mathrm{Nu} = \left(2^4 \frac{\mathrm{Ra}}{\mathrm{Ra}_{\mathrm{cr}}}\right)^{\frac{1}{3}}, \tag{S-2}$$

where Ra is the Rayleigh number and $\mathrm{Ra}_{\mathrm{cr}}$ is the critical value of the Rayleigh number (Turcotte & Schubert, 2014). The Rayleigh number is defined as:

$$\mathrm{Ra} = \frac{\alpha\,\rho\,g\,\Delta T\,d^3}{\kappa\,\eta}, \tag{S-3}$$

where α is the thermal expansivity coefficient, g is the surface gravitational acceleration, ΔT is the temperature difference between the limiting surface and the limit of the conduction lid of thickness d, closest to the former. In addition, $\kappa = k\;(c\,\rho)^{-1}$ is the thermal diffusivity and η is the dynamical viscosity.

Equating Equations (S-1) and (S-2) leads to:

$$q^{\mathrm{conv}} = \left(2^4\,\frac{\mathrm{Ra}}{\mathrm{Ra}_{\mathrm{cr}}}\right)^{\frac{1}{3}} q^{\mathrm{cond}}. \tag{S-4}$$

In order to derive the expression of the conductive thermal flux, consider the volume enclosed by two concentric spherical surfaces, which we assume it is filled with a solid material. The inner spherical surface has radius R_{in} and it is at temperature T_{in}, while the outer one has radius R_{out} and it is at temperature T_{out} (see Figure S1) which is assumed to be less than T_{in} ($T_{\mathrm{out}} < T_{\mathrm{in}}$).

If we assume that heat transfers within the material enclosed by the concentric spherical surfaces by conduction, then the temperature profile inside the volume can be found by virtue of the Fourier's law:

$$\mathbf{q} = -\,k\,\nabla T \tag{S-5}$$

where k is the thermal conductivity of the material and T is the temperature. In the following, some simplifying assumption will be considered. First, we will consider the temperature distribution in the steady state. In consequence, the time derivative of the energy density is equal to zero and the equation expressing the energy conservation law:

$$\frac{\partial u}{\partial t} + \nabla \cdot \mathbf{q} = \varrho\left(\mathbf{r}, t\right), \tag{S-6}$$

becomes:

$$\nabla \cdot \mathbf{q} = 0. \tag{S-7}$$

In addition, we will assume that heat flows radially outwards the hollow sphere. This implies that $\mathbf{q} = q_r \hat{\mathbf{r}}$, where $\hat{\mathbf{r}}$ is the corresponding versor that is perpendicular to the spherical surfaces at each point and its sense is outwards the aforementioned surface. Taking this assumption into account, Equation (S-7) can be rewritten as:

$$\frac{1}{r^2}\frac{\mathrm{d}}{\mathrm{d}r}\left[r^2\, q_r(r)\right] = 0. \tag{S-8}$$

Similarly, Fourier law takes the form:

$$q_r = -\,k\,\frac{\mathrm{d}T}{\mathrm{d}r}. \tag{S-9}$$

Then, by inserting Equation (S-9) into Equation (S-8) and simplifying we obtain:

$$\frac{\mathrm{d}}{\mathrm{d}r}\left[r^2\,\frac{\mathrm{d}T(r)}{\mathrm{d}r}\right] = 0. \tag{S-10}$$

The solution of Equation (S-10) considering the boundary conditions $T(R_{\mathrm{in}}) = T_{\mathrm{in}}$ and $T(R_{\mathrm{out}}) = T_{\mathrm{out}}$ is (Carslaw & Jaeger, 1959):

$$T(r) = \frac{R_{\mathrm{out}}\,T_{\mathrm{out}}\left(r - R_{\mathrm{in}}\right) + R_{\mathrm{in}}T_{\mathrm{in}}\left(R_{\mathrm{out}} - r\right)}{\left(R_{\mathrm{out}} - R_{\mathrm{in}}\right) r}. \tag{S-11}$$

By virtue of Equation (S-9) we have:

$$q(r) = k\frac{(T_{\mathrm{in}} - T_{\mathrm{out}})}{(R_{\mathrm{out}} - R_{\mathrm{in}})}\frac{R_{\mathrm{out}}\,R_{\mathrm{in}}}{r^2}. \tag{S-12}$$

Thus, the heat flux through the inner spherical surface, crossing it radially outwards, is:

$$q(R_{\mathrm{in}}) = k\frac{(T_{\mathrm{in}} - T_{\mathrm{out}})}{d}\frac{1}{1 - z}, \tag{S-13}$$

where we have expressed R_{in} as $R_{\mathrm{out}} - d$, where d is the thickness of the hollow sphere (Figure S1), and defined $z = d/R_{\mathrm{out}}$. Analogously, the heat flux through the outer sphere is:

$$q(R_{\mathrm{out}}) = k\frac{(T_{\mathrm{in}} - T_{\mathrm{out}})}{d}\,(1 - z)\,. \tag{S-14}$$

In practice $z \ll 1$ and, consequently, Equation (S-13) can be rewritten as:

$$q(R_{\mathrm{in}}) = k\frac{(T_{\mathrm{in}} - T_{\mathrm{out}})}{d}\left(1 + z + z^2 + \ldots\right), \tag{S-15}$$

It is very common in the specialized literature to consider only the zeroth order of approximation in both Equation (S-14) and Equation (S-15). In our work we will follow the same tendency, but we would like to pose the question to which extent the aforementioned approximation remains valid and to leave the discussion to a future work. In consequence, as long as the approximation $z \ll 1$ remains valid in Equations (S-14) and (S-15), the expression of the conductive heat flow corresponding to conductive heat transfer through a slab can be considered:

$$q^{\mathrm{cond}} = k\frac{\Delta T}{d}. \tag{S-16}$$

Insertion of Equations (S-3) and (S-16) into Equation (S-4) leads to:

$$q^{\mathrm{conv}} = k\left(\frac{2^4}{\mathrm{Ra}_{\mathrm{cr}}}\frac{\alpha\,\rho\,g\,\Delta T}{\kappa\,\eta}\right)^{\frac{1}{3}}\Delta T. \tag{S-17}$$

In the following, the superscript “conv” can be omitted. By comparing Equations (S-16) and (S-17) we can obtain an expression of the conductive lid thickness:

$$d = \left(\frac{\mathrm{Ra}_{\mathrm{cr}}\,\kappa\,\eta}{2^4\alpha\,\rho\,g\,\Delta T}\right)^{\frac{1}{3}}. \tag{S-18}$$

Thus, the right hand side of Equation (S-17) can be replaced by the right hand side of Equation (S-16) with d given by Equation (S-18).

If we assume that $T_1 > T_{\rm iso} > T_2$ in Figure S2, then the incoming heat flux from below is given by Equation (S-17) in which $\Delta T = \Delta T_1 = T_1 - T_{\rm iso}$, where $T_{\rm iso}$ is the isothermal temperature. The out-coming heat flux is also given by Equation (S-17) but $\Delta T = \Delta T_2 = T_{\rm iso} - T_2$.

Thus, the expressions of the heat fluxes inside the Earth, which are the outgoing heat flux from the core and the heat fluxes incoming into and outgoing from the mantle, can be obtained in a straightforward fashion.

Text S2. Expression of the radioactive heat production rate

The expression of $H(t)$ was taken from the work by Turcotte and Schubert (2014), which we reproduce here.

$$\begin{aligned} H(t) = 0.9928\, C_0^{\rm U} H_0\left({}^{238}{\rm U}\right) \exp\left[-\frac{\ln 2}{\tau_{\frac{1}{2}}\left({}^{238}{\rm U}\right)}(t-t_0)\right] \\ + 0.0071\, C_0^{\rm U} H_0\left({}^{235}{\rm U}\right) \exp\left[-\frac{\ln 2}{\tau_{\frac{1}{2}}\left({}^{235}{\rm U}\right)}(t-t_0)\right] \\ + C_0^{\rm Th} H_0\left({}^{232}{\rm Th}\right) \exp\left[-\frac{\ln 2}{\tau_{\frac{1}{2}}\left({}^{232}{\rm Th}\right)}(t-t_0)\right] \\ + 1.19\times 10^{-4} C_0^{\rm K} H_0\left({}^{40}{\rm K}\right) \exp\left[-\frac{\ln 2}{\tau_{\frac{1}{2}}\left({}^{40}{\rm K}\right)}(t-t_0)\right]. \end{aligned} \quad \text{(S-19)}$$

where C_0 and H_0 are the concentration and heat production rate per unit mass of each isotope at instant t_0, while $\tau_{\frac{1}{2}}$ is the corresponding half-life. In Table S1 we reproduce the values given in the work by Turcotte and Schubert (2014).

Text S3. Rheological models

The rheological response of a solid body is described by the complex Love numbers:

$$K_{\rm I}(l,\omega_{lmpq}) = -\frac{3}{2}\frac{1}{l-1}\frac{B_l\,\Im\left[\bar{J}(\chi)\right]\,{\rm sgn}\left(\omega_{lmpq}\right)}{\left(\Re\left[\bar{J}(\chi)\right]+B_l\right)^2+\left(\Im\left[\bar{J}(\chi)\right]\right)^2}, \quad \text{(S-20)}$$

in which $J(\chi)$ is defined by:

$$\bar{J}(\chi) = \int_0^\infty \dot{J}(t-t')\exp\left[-\mathrm{i}\chi(t-t')\right]\mathrm{d}t', \tag{S-21}$$

where the over-dot means differentiation with respect to t' and $\mathrm{i} = \sqrt{-1}$ is the imaginary unit. The particular form of the kernel $J(t-t')$ depends on the particular rheological model considered. However, it is generally given by:

$$J(t-t') = J(0)\,\Theta(t-t') + \text{viscous and hereditary terms}, \tag{S-22}$$

where $J(0)$ is the instantaneous value of the compliance which, in its turn, is the reciprocal value of the instantaneous rigidity $\mu(0)$, and $\Theta(t-t')$ is the Heaviside step function (Efroimsky, 2012).

The first term on the right hand side of Equation (S-22) describes the instantaneous elastic response in deformation of the body under stress. However, the general rheological response of a real solid body is a mixture of elastic and anelastic behavior. The latter includes viscous and hereditary behaviors.

The complex compliance is obtained from the *constitutive equation*, which relates stress and strain. In a linear medium, assumed to be homogeneous, incompressible and isotropic, the relationship between the components of the stress tensor and the strain tensor is, in general terms, given by:

$$2\,\bar{u}_{\gamma\nu}(\chi) = \bar{J}(\chi)\,\bar{\sigma}_{\gamma\nu}(\chi), \tag{S-23}$$

where $\bar{u}_{\gamma\nu}(\chi)$ and $\bar{\sigma}_{\gamma\nu}(\chi)$ are the complex counterparts of the strain and stress tensors, respectively (Efroimsky, 2012).

In our work, we will consider three rheological models to describe tidal dissipation within Earth's mantle, namely the Maxwell, the Burgers and Maxwell-Andrade models.

The Maxwell, Kelvin-Voigt and Burgers rheological models are typical examples of models used to describe different types of viscoelastic behavior of a solid body. The first one is represented as a dashpot and a spring connected in series. The second one is represented as a dashpot and a spring connected in parallel. These two models differ in at least two aspects. On one hand, after being deformed a body whose rheological behavior is characterized by the Maxwell model can not recover is shape. On the contrary, a body whose rheological behavior is described by the Kelvin-Voigt model, do recover its shape. On the other hand, in a Maxwell configuration, the applied stress acting on the spring and on the dashpot are equal, while the total deformation is the sum of the deformations of each of the aforementioned components.

The Burgers model can be thought as a Kelvin-Voigt element connected in series with a Maxwell element. It worth to note that the viscosity of the dashpot in the Kelvin-Voigt element has a different meaning from that of the viscosity of the dashpot in the Maxwell element (Renaud & Henning, 2018).

The last rheological model to be considered is that of Maxwell-Andrade. It is schematically similar to the Burgers model, but has the fundamental difference that the viscosity of the dashpot and the compliance (or rigidity) of the spring in the Kelvin-Voigt element are not fixed but are variable in order to allow for the hereditary reaction behavior (Efroimsky, 2012; Renaud & Henning, 2018). As a consequence of this, the Burgers element does not exactly recover its original form, i.e. there is a certain “hysteresis”. The origin of the latter is due to dislocations and vacancy flow within the material that responds according to this rheology.

Concerning the expression of the complex creep function, $\bar{J}(\chi)$, which is given in general terms by Equation (S-21), in the following we will present its specific from for each rheology in a suitable form for its translation into a computer code.

For the Maxwell model, the expression of $J(t-t')$, which was given in its general form in Equation (S-22), is (Efroimsky, 2012):

$$J(t-t') = \left[J + (t-t')\frac{1}{\eta}\right]\Theta(t-t'). \tag{S-24}$$

Inserting Equation (S-24) in Equation (S-21), and performing the required mathematical operations, we obtain:

$$\bar{J}\left(\chi\right) = J - \frac{\mathrm{i}}{\chi\,\eta}. \tag{S-25}$$

The real and imaginary parts of the right hand side of Equation (S-25) are evidently:

$$\Re\left[\bar{J}(\chi)\right] = J \tag{S-26a}$$

$$\Im\left[\bar{J}(\chi)\right] = -\frac{1}{\chi\,\eta}. \tag{S-26b}$$

The next step would be to insert Equations (S-26) into Equations (S-20). However, the presence of the tidal frequency in the denominator on the right hand side of Equation (S-26b) can cause numerical instabilities, given the possibility that χ can become zero when the considered rotating body crosses or gets captured in a spin-orbit resonance (Efroimsky, 2012). In order to avoid this numerical difficulty, we can define the dimensionless complex compliance $\mathcal{J}(\chi)$ as:

$$\mathcal{J}(\chi) = \eta\,\chi\,\bar{J}(\chi). \tag{S-27}$$

By multiplying and dividing the right hand sides of Equations (S-20) by $\eta^2\chi^2$, we can express the tidal quality functions in terms of the dimensionless complex compliance:

$$K_{\mathrm{I}}(l,\omega_{lmpq}) = -\frac{3}{2}\frac{1}{l-1}\frac{B_l\,\eta\,\chi\,\Im\left[\mathcal{J}(\chi)\right]\operatorname{sgn}\left(\omega_{lmpq}\right)}{\left(\Re\left[\mathcal{J}(\chi)\right]+B_l\,\eta\,\chi\right)^2+\left(\Im\left[\mathcal{J}(\chi)\right]\right)^2}. \tag{S-28}$$

Using Equation (S-25) and Equation (S-27), the dimensionless creep response function for the Maxwell rheology is:

$$\mathcal{J}(\chi) = J\,\eta\,\chi - \mathrm{i}, \tag{S-29}$$

whose real and imaginary parts are:

$$\Re\left[\mathcal{J}(\chi)\right] = J\,\eta\,\chi \tag{S-30a}$$

$$\Im\left[\mathcal{J}(\chi)\right] = -1. \tag{S-30b}$$

Inserting Equations (S-30) into Equations (S-28) we obtain:

$$K_{\mathrm{I}}(l,\omega_{lmpq}) = \frac{3}{2}\frac{1}{l-1}\frac{B_l\,\eta\,\chi\operatorname{sgn}\left(\omega_{lmpq}\right)}{\left(J+B_l\right)^2\eta^2\,\chi^2+1}. \tag{S-31}$$

The rheology of a body described by the Maxwell model behaves as a elastic solid at high frequencies ($\chi\,\eta\,J \gg 1$). On the contrary, at low frequencies, it behaves as a viscous solid body ($\chi\,\eta\,J \ll 1$). Consequently, this kind of behavior has the particular feature of underestimate tidal dissipation at high frequencies. In order to overcome this inconvenience, more realistic rheologies can be considered such as the Burgers and Maxwell-Andrade models.

The complex compliance function corresponding to the Burgers model is given by (Renaud & Henning, 2018):

$$\bar{J}\,(\chi) = J - \frac{\mathrm{i}}{\eta\,\chi} + J_{\mathrm{R}}\left(\frac{1-\mathrm{i}\,J_{\mathrm{R}}\,\eta_*\,\chi}{1+\left(J_{\mathrm{R}}\,\eta_*\,\chi\right)^2}\right). \tag{S-32}$$

For the sake of reducing the number of free parameters, we follow the work by Renaud and Henning (2018), who expressed the relaxed compliance, J_{R}, and the Kelvin-Voigt viscosity, η_*, in terms of the unrelaxed compliance, J, and the Maxwell viscosity, η, as follows:

$$J_{\mathrm{R}} = \zeta_{\mathrm{J}}\, J, \tag{S-33a}$$

y

$$\eta_* = \zeta_\eta\, \eta. \tag{S-33b}$$

For the Earth's mantle, the parameters ζ_{J} and ζ_η are taken equal to 0.2 and 0.02, respectively (Renaud & Henning, 2018).

The corresponding expression of the dimensionless complex compliance is:

$$\mathcal{J}(\chi) = J\,\eta\,\chi - \mathrm{i} + \zeta_{\mathrm{J}}\,J\,\eta\,\chi\left(\frac{1-\mathrm{i}\,\zeta_{\mathrm{J}}\,\zeta_\eta\,J\,\eta\,\chi}{1+\left(\zeta_{\mathrm{J}}\,\zeta_\eta\,J\,\eta\,\chi\right)^2}\right), \tag{S-34}$$

while its real and imaginary parts are:

$$\Re\left[\mathcal{J}(\chi)\right] = J\,\eta\,\chi\left(1+\frac{\zeta_{\mathrm{J}}}{1+\left(\zeta_{\mathrm{J}}\,\zeta_\eta\,J\,\eta\,\chi\right)^2}\right) \tag{S-35a}$$

$$\Im\left[\mathcal{J}(\chi)\right] = -\left(1+\frac{\zeta_\eta\left(\zeta_{\mathrm{J}}\,J\,\eta\,\chi\right)^2}{1+\left(\zeta_{\mathrm{J}}\,\zeta_\eta\,J\,\eta\,\chi\right)^2}\right). \tag{S-35b}$$

These expressions combined with Equations (S-28) deliver the values of $K_{\mathrm{I}}\left(l, \omega_{lmpq}\right)$.

Similarly, the complex creep response function corresponding to the Maxwell-Andrade model is given by:

$$\bar{J}(\chi) = J - \frac{\mathrm{i}}{\eta\,\chi} + \frac{J^{1-\alpha}}{\left(\mathrm{i}\,\zeta_{\mathrm{A}}\,\eta\,\chi\right)}\Gamma\left(1+\alpha\right), \tag{S-36}$$

where α is known as Andrade's parameter and ζ_{A} is identified with the ratio between the characteristic times of the Maxwell-Andrade rheology (τ_{A}) and that of the viscoelastic response (τ_{M}). In general, due to the current lack of knowledge about this particular aspect, it is common to set $\zeta_{\mathrm{A}} = 1$, which implies $\tau_{\mathrm{A}} = \tau_{\mathrm{M}}$. This last equality is approximately true for relatively low stresses, such as the ones we have in this kind of study (Castillo-Rogez et al., 2011). On the other hand, Karato and Spetzler (1990) point out that the anelastic dissipation mechanism is effective in the Earth's mantle up to the limit frequency $\chi_0 \simeq 1$ year^{-1}. At lower frequencies, this mechanism is less efficient resulting in viscoelastic behavior. That is, at low frequencies the mantle behaves like a Maxwell solid. Consequently, for frequencies higher than χ_0, the anelasticity is the dominant dissipation mechanism and, therefore, in such a frequency regime the aforementioned equality is satisfied (Efroimsky, 2012).

Concerning the Andrade parameter, α, it should be noted that the values it assumes (which is specific to each material) are always in the interval $[0.14, 0.4]$ for all minerals, including ice, which constitutes a surprising fact (Efroimsky, 2012). The lower values of the interval correspond to materials at high temperatures or semi-molten and the higher values correspond to colder rocks and ices.

The dimensionless complex compliance function for Maxwell-Andrade rheology is given by:

$$\mathcal{J}\left(\chi\right) = J\,\eta\,\chi - \mathrm{i} + \frac{J\,\eta\,\chi}{\left(\zeta_{\mathrm{A}}\,J\,\eta\,\chi\right)^{\alpha}} \exp\left(-\mathrm{i}\frac{\pi}{2}\alpha\right)\Gamma\left(1+\alpha\right). \tag{S-37}$$

Then, the real and imaginary parts of $\mathcal{J}\left(\chi\right)$ for the same rheology are given by:

$$\Re\left[\mathcal{J}(\chi)\right] = J\,\eta\,\chi + \frac{J\,\eta\,\chi}{\left(\zeta_{\mathrm{A}}\,J\,\eta\,\chi\right)^{\alpha}}\Gamma\left(1+\alpha\right)\cos\left(\frac{\pi}{2}\alpha\right), \tag{S-38a}$$

$$\Im\left[\mathcal{J}(\chi)\right] = -1 - \frac{J\,\eta\,\chi}{\left(\zeta_{\mathrm{A}}\,J\,\eta\,\chi\right)^{\alpha}}\Gamma\left(1+\alpha\right)\sin\left(\frac{\pi}{2}\alpha\right). \tag{S-38b}$$

In the case that the response of certain material that makes up a celestial body is modeled with this rheology, the expressions given in Equation (S-38) have to be combined with Equations (S-28) in order to evaluate the tidal quality function $K_{\mathrm{I}}\left(l, \omega_{lmpq}\right)$.

References

Carslaw, H. S., & Jaeger, J. C. (1959). *Conduction of heat in solids.* Oxford Science publications.

Castillo-Rogez, J. C., Efroimsky, M., & Lainey, V. (2011). The tidal history of iapetus: Spin dynamics in the light of a refined dissipation model. *Journal of Geophysical Research: Planets*, *116*(E9), n/a–n/a. Retrieved from `http://dx.doi.org/10.1029/2010JE003664` (E09008) doi: 10.1029/2010JE003664

Efroimsky, M. (2012, March). Bodily tides near spin-orbit resonances. *Celestial Mechanics and Dynamical Astronomy*, *112*, 283-330. doi: 10.1007/s10569-011-9397-4

Karato, S., & Spetzler, H. A. (1990, November). Defect microdynamics in minerals and solid state mechanisms of seismic wave attenuation and velocity dispersion in the mantle. *Reviews of Geophysics*, *28*, 399-421. doi: 10.1029/RG028i004p00399

Renaud, J. P., & Henning, W. G. (2018, apr). Increased tidal dissipation using advanced rheological models: Implications for io and tidally active exoplanets. *The Astrophysical Journal*, *857*(2), 98. Retrieved from `https://doi.org/10.3847/1538-4357/aab784` doi: 10.3847/1538-4357/aab784

Stacey, F. D., & Davis, P. M. (2008). *Physics of the earth* (Fourth ed.). Cambridge University Press.

Turcotte, D., & Schubert, G. (2014). *Geodynamics* (3rd ed.). Cambridge University Press.

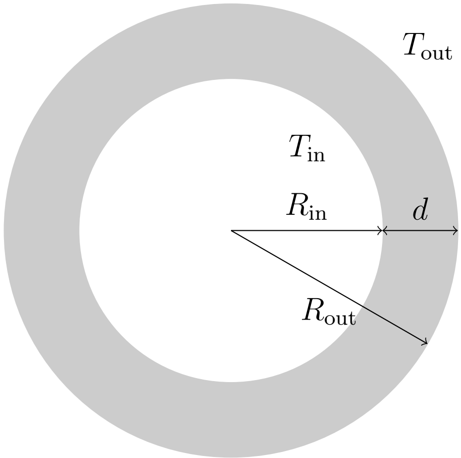

Figure S1. Schematic representation of a hollow sphere with the representative parameters used to derive the thermal flux from the internal surface to the external surface through the volume enclosed by both surfaces.

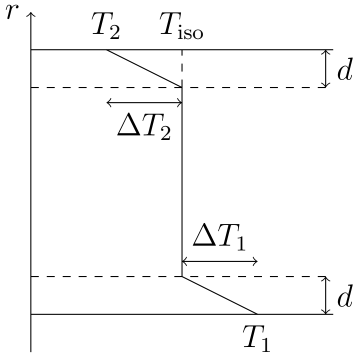

Figure S2. Vertical temperature profile in a setting where heat transport is dominated by convection.

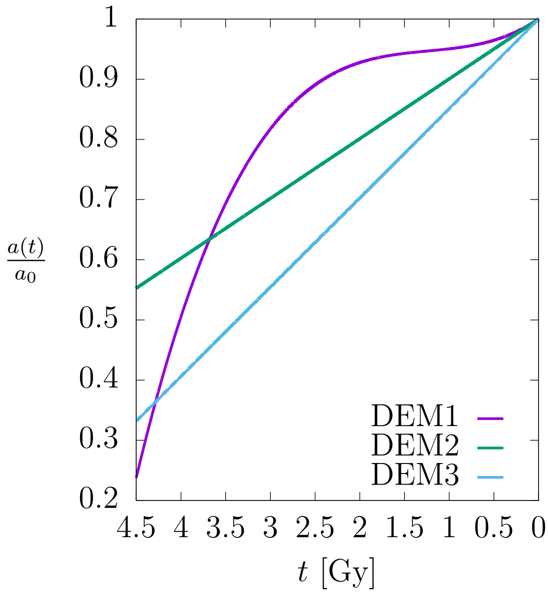

Figure S3. Plots of the three different assumed dynamical evolution models (DEMs) of the major semiaxis of the Moon's orbit

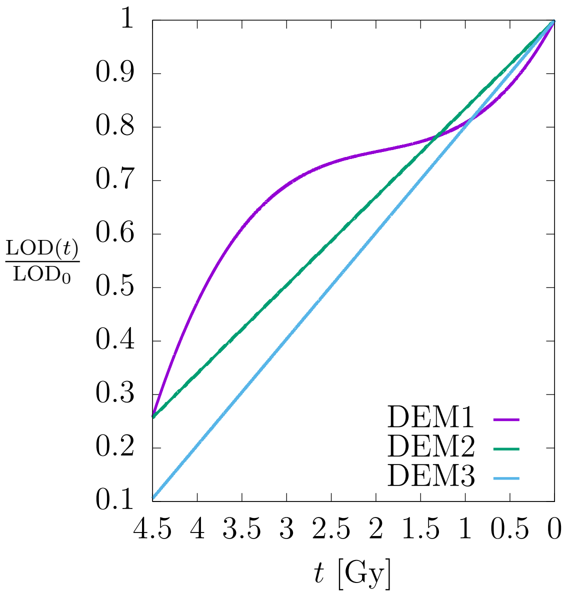

Figure S4. Plots of the three different assumed dynamical evolution models (DEMs) of the Earth's LOD.

Table S1. Thermally relevant radioactive isotopes together with the corresponding values of the parameters needed to compute the respective heat production rate per unit mass (Turcotte & Schubert, 2014).

Isotope	H_0 [W kg^{-1}]	$\tau_{\frac{1}{2}}$ [yr]	C_0 [kg kg^{-1}]
^{238}U	9.46×10^{-5}	4.47×10^{9}	30.8×10^{-9}
^{235}U	5.69×10^{-4}	7.04×10^{8}	0.22×10^{-9}
U	9.81×10^{-5}		31.0×10^{-9}
^{232}Th	2.64×10^{-5}	1.40×10^{10}	124×10^{-9}
^{40}K40	2.92×10^{-5}	1.25×10^{9}	36.9×10^{-9}
K	3.48×10^{-9}		31.0×10^{-5}

Table S2. Constants, physical and orbital parameters of the Earth-Moon system gathered from the works by (Stacey & Davis, 2008) and (Turcotte & Schubert, 2014).

Symbol	Value
G	6.67408×10^{-11}kg^{-1} m^3 s^{-2}
R_{gas}	8.31447 J K^{-1} mol^{-1}
$M_{\oplus}$	5.9722×10^{24}kg
$R_{\oplus}$	6.371×10^{6} m
R_{c}	3.480×10^{6} m
$M_{☾}$	7.342×10^{22} kg
ξ	$\frac{1}{3}$
μ	8.0×10^{10} Pa
η_{ref}	4.5×10^{21} Pa s
T_{ref}	1600.0 K
T_{s}	300.0 K
$\mathrm{Ra}_{\mathrm{cr}}$	1000
E^{*}	3.0×10^{5} J mol^{-1}
α	0.2
a	3.844×10^{8} m
e	0.0549
i	$\sim 23.5°$
P_{orb}	27.322 days

Table S3. Physical parameters and their corresponding numerical value for the core and mantle gathered from the works by (Stacey & Davis, 2008) and (Turcotte & Schubert, 2014).

Symbol	Unit	Core	Mantle
α	K^{-1}	1.0×10^{-5}	1.5×10^{-5}
ρ	$kg\,m^{-3}$	1.076×10^{4}	4.5×10^{3}
g	$m\,s^{-2}$	7.0	10.0
κ	$m^2 s^{-1}$	6.0×10^{-6}	1.0×10^{-6}
k	$W\,K^{-1} m^{-1}$	36.0	6.0
ν	$m^2\,s^{-1}$	1.0	Variable